BNL--52327

DE92 016754

BREAKUP OF MOLTEN ALUMINUM JETS INJECTED INTO WATER

*G.A. Greene, C.C. Finfrock, C.E. Schwarz, and **M.L. Hyder

January 1992

*EXPERIMENTAL HEAT TRANSFER AND FLUID DYNAMICS GROUP
DEPARTMENT OF NUCLEAR ENERGY
BROOKHAVEN NATIONAL LABORATORY, ASSOCIATED UNIVERSITIES, INC.
UPTON, LONG ISLAND, NEW YORK 11973

**SAFETY ANALYSIS GROUP
SAVANNAH RIVER LABORATORY
WESTINGHOUSE SAVANNAH RIVER COMPANY
AIKEN, SOUTH CAROLINA 29808

UNDER CONTRACT NO. DE-AC02-76CH00016 WITH THE
UNITED STATES DEPARTMENT OF ENERGY

DISCLAIMER

Printed in the United States of America
Available from
National Technical Information Service
U.S. Department of Commerce
5285 Port Royal Road
Springfield, VA 22161

NTIS price codes:
Printed Copy: A04; Microfiche Copy: A01

ABSTRACT

A series of eighteen tests were performed to investigate the behavior of a molten jet of aluminum as it penetrates a deep pool of subcooled water. Jet penetration lengths required for breakup were found to agree with an existing model. Debris size and density were measured and are presented as a function of the jet diameter and water pool temperature. For those tests that exhibited the ability to spread across the steel baseplate under the water, the melt spreading behavior is compared to the existing melt spreading correlation. In the jet mode of melt-water contact, no explosive interactions were observed in these tests. Due to the nearly prototypical nature of these tests, it appears reasonable to conclude that gamma heating of non-fuel components during the DEGB-LOCA would, at worst, benignly melt some aluminum components in the reactor tank, resulting in large particles or debris formations which would remain in the tank and be coolable.

EXECUTIVE SUMMARY

The objectives of the present study are to perform a series of experiments intended to assist in the resolution of the γ-heating issue. The tests are non-prototypic in the strict sense, but close to prototypic where practical and feasible. Parameters of the tests which are representative or prototypic of expected γ-heating conditions or bound those conditions are water temperature, water pool depth, melt composition, melt temperature, and jet or pour diameter. Note that the melt composition is prototypic of septifoils, thimbles, and housings. Aspects of the tests which are not prototypic are the water pool flow patterns and specific component geometry. The specific objective of these tests is to create pours or jets of molten aluminum of small diameter into water pools in order to simulate the melt-water contact mode that is expected under γ-heating conditions. Measurements will be made of jet breakup length in the water pool, debris size, debris density, and debris spreading and coolability. The dependance of these processes upon water temperature and depth will be established.

An A frame gantry has been constructed from prefabricated metal framing channel to carry the necessary equipment to pour molten aluminum. The ridge beam of the gantry spans eight feet and is at an elevation of approximately seven feet. Vertical struts extend downward from this ridge beam to carry a melt crucible mounted on an axle. Horizontal struts extend forward from the legs of the gantry and carry a frame which holds a funnel and nozzle assembly forward of, and slightly below the crucible. When melt is to be delivered, the pot axle is rotated, pouring the melt from the crucible to the funnel which delivers the melt to the test pool. The crucibles are fabricated of type 304 stainless steel and are electrically heated. Sections of schedule 5 or 10 stainless steel pipe of appropriate diameter are cut to the required length to give the volume desired, and flat, square plates are welded on one end. Clamshell type electric resistance elements of the proper dimensions are mounted on the crucibles and typically backed up with one to three inches of ceramic fiber insulation as needed. The funnel and nozzle assembly is also fabricated from type 304 stainless steel. It consists of a conical upper section which terminates in a flange which can be fitted with stainless steel nozzles of various diameters. The test pool is located beneath the funnel. The pool is fabricated from acrylic plastic sheet, hot gas welded into a square tank 30" w x 30" l x 24" h. The tank is also equipped with discharge and return fittings that allow connection to an external electric water heater and pump assembly to provide the desired water temperature. A 3/16" thick type 304 stainless steel plate resides on the floor of the tank and protects the acrylic from damage by hot aluminum.

When the required melt, water, and funnel temperatures are reached, non-essential personnel are cleared from the area and a secure perimeter is established and maintained during run execution. The aluminum and water are both stirred to insure uniform temperatures. The data acquisition system is switched from monitor mode to acquisition mode and is held to be started in concert with the pour. The insulating covers are removed from the crucible and funnel, the duration-of-pour light cell is activated, the video camera and lights are activated, and the operators assume their positions at the data acquisition computer and the crucible pouring controls. On command, the data acquisition is initiated and the aluminum is rapidly transferred

to the funnel and nozzle assembly. The duration of pour is determined by the nozzle diameter and gravitational head of aluminum.

A series of eighteen experiments were executed in this series of tests to examine the possible interactions as a small diameter jet of molten aluminum penetrates a deep water pool. The following observations and conclusions were made in the course of these investigations. No aluminum-water steam explosions occurred in any of these tests. It appears from these tests that the contact mode between aluminum and water is critical in determining whether an aluminum-water steam explosion will occur. These tests employed the jet-entry mode exclusively. The jet breakup length agrees with existing models quite well. In cold water pools, molten aluminum jets break up into particles and form loose debris beds. In hot water pools, the particles from the jet breakup do not completely freeze prior to piling up at the bottom of the pool. There they form clumps of particles and even reform into solid, non-porous formations. Virtually no particulate debris smaller than 3 mm was formed in these tests. At the highest water pool temperatures, the aluminum melt actually spread radially along the bottom of the pool on the stainless steel base. The debris that formed into particles was less dense than solid aluminum. This would make these debris beds easily leveled by crossflow currents, enhancing debris coolability.

TABLE OF CONTENTS

FIGURES

LIST OF FIGURES (Cont'd)

LIST OF TABLES

NOMENCLATURE

$c_{p,j}$	jet specific heat
$c_{p,w}$	water specific heat
d_j	jet diameter
h_{fg}	latent heat of vaporization, water
h_{fs}	latent heat of fusion, melt
H_w	water depth
Ja	Jakob number ($\equiv c_{p,w}\,\Delta T_{sub}\,/h_{fg}$)
L	jet breakup length
L^*	dimensionless jet breakup length, (defined in Equation 1)
M	mass of debris
N_{sp}	dimensionless spreading parameter $\left[\equiv \frac{(M/\rho_j)^{1/3}}{H_w} \cdot \frac{\rho_j}{\rho_c} \cdot \frac{h_{fs}}{h_{fg}} \cdot \frac{1+Sf}{1+Ja} \right]$
Sf	Stefan number ($\equiv c_{p,j}\,\Delta T_{super}\,/h_{fs}$)
t	average thickness of spreading debris
t^*	dimensionless melt thickness ($\equiv t/(2\sigma/\rho_j\, g)^{1/2}$)
T_w	water temperature
ΔT_{sub}	water subcooling below saturation
ΔT_{super}	melt superheat above fusion temperature
u_j	jet velocity at water surface
We	Weber number, (defined in Equation 2)

NOMENCLATURE (Cont'd)

ρ_c	water density
ρ_j	melt jet density
σ	interfacial tension

1. INTRODUCTION

1.1 Background

An intensive effort has been underway for several years at WSRC to accomplish improvements in operations, maintenance, facilities, technical specifications, training, and safety required to support the restart of the K-reactor. A major component of the restart effort, and possibly the most complicated and important, has been the thermal-hydraulics analytical and experimental program whose mission it has been to establish a technically sound operating power for the reactor such that there would be no fuel damage in the event of a design basis accident, a DEGB-LOCA.

The ongoing thermal-hydraulics power limits program at WSRC has focused its efforts at the development and verification of an analytical methodology and supporting data bases for acceptance criteria for two phases of the DEGB-LOCA. These are the flow instability (FI) phase and the phase during operation of the emergency cooling system (ECS phase). For FI, it is required that the lead assemblies satisfy an upper limit Stanton number criterion in order to ride out the pipe break and not enter into a Ledinegg flow instability. For ECS, it is required that the air-water two phase flow be sufficient to cool the fuel assemblies below the local saturation temperature of the coolant. On the basis of FLOWTRAN code calculations, it has been established that a restart power of approximately 36% of historical full power would be sufficiently low to ensure compliance with both of these phenomenologically based acceptance criteria.

It is during the ECS phase of the LOCA that a two-phase air-water mixture would be pumped through the primary system to cool the core. As a result of the air in the system, the pump performance would be degraded and may not keep up with coolant loss through the break location. The inlet plenum would become stratified and the liquid level in the tank would drop until the reactor tank water level stabilized at a depth of 1-2 feet from the bottom. Nevertheless, the fuel assemblies would be internally cooled and remain protected.

The loss of moderator in the tank would ensure neutronic shutdown and the core would be stabilized at decay heat power. However, the empty tank would expose non-fuel components to decay heat γ-energy that would otherwise be absorbed in the moderator if the reactor tank were full of water. Since, with one exception, the non-fuel components would have no forced convective cooling, i.e., they are normally cooled by the relatively stagnant tank moderator, these components would be vulnerable to overheating and possibly melting or structural failure.

The non-fuel components in the reactor tank that are vulnerable to overheating by absorption of decay heat γ-energy include the tank wall, USH, control rods and septifoils, safety rods and thimbles, and blanket assemblies. The septifoils do retain some forced cooling (core flow is down but septifoil cooling, which is drawn from the heat exchanger discharge, is in the upward direction); however, since the septifoils are perforated and lose coolant flow to the tank along their vertical axes, the effectiveness of this cooling is not certain. Current assessments

suggest that most non-fuel components would heat up but not fail due to melting. Some components, such as the control rods and thimbles, have been identified as the most vulnerable. Estimates that have been made indicate possible heat up rates as high as 80°C/min., which would lead to component melting in as little as six minutes following tank draining. In some instances, structural failure could occur during heat up; in other instances, gradual component melting would ensue. The most vulnerable components are, of course, those constructed of aluminum, such as the thimbles and septifoils. However, due to the large specific heat and latent heat of freezing/melting of aluminum, any melting would be expected to be gradual, not wide spread and massive.

Such an event (DEGB-LOCA) has, of course, not occurred during the operating experience with heavy water production reactors at WSRC. Therefore, it is not possible to predict the scenario of events and consequences of the γ-heating effect from experience. As is not uncommon with respect to predicting the consequences of heretofore unexperienced transients or hypothetical accidents in reactor systems, worst case scenarios are usually created in an effort to be conservative. These worst case scenarios can only be overcome by relevant data and reliable analyses and engineering judgement. In the γ-heating issue, events which have been suggested as being of potential concern range from Al/H_2O steam explosions in the reactor tank with the potential to cause sufficient mechanical damage to compromise the ECS function, to generation of a sufficient amount of fine particulate aluminum debris, either from the Al/H_2O explosion or some other more benign melt fragmentation process, debris which could be transported through the primary system, further degrading the pump function and possibly causing blockages in the primary heat exchangers or fuel assembly inlets.

In either event, the ECS flow may be compromised, resulting in a higher potential for fuel damage. This could create a situation in which the γ-heating effect could become the most limiting consideration in establishing the restart power for the K-reactor, more limiting than either FI or ECS.

1.2 Objectives

The objectives of the present study are to perform a series of experiments intended to assist in the resolution of the γ-heating issue. These experiments are scoping tests by nature, intended to be completed in the near term using existing test facilities for studies with molten aluminum. The tests are non-prototypic in the strict sense, but close to prototypic where practical and feasible.

Aspects of the tests which are representative or prototypic of expected γ-heating conditions or bound those conditions are listed below:

- water temperature : 20-70°C
- water pool depth : 25-50 cm
- melt composition : aluminum

- melt temperature : ~700°C
- jet or pour diameter : 1/8, 1/4, 1/2 inch

Note that the melt composition is prototypic of septifoils, thimbles, and housings. Aspects of the tests which are not prototypic are listed below:

- water pool flow patterns
- specific component geometry

The specific objectives of these tests are to create pours or jets of molten aluminum of small diameter into water pools in order to simulate the melt-water contact mode that is expected under γ-heating conditions. A prime objective is to look for melt-water explosive events and the conditions which may promote these events. Measurements will be made of jet breakup length in the water pool, debris size, debris density, and debris spreading and coolability. The dependance of these processes upon water temperature and depth will be established.

2. EXPERIMENTAL APPARATUS AND PROCEDURES

2.1 Apparatus

An A frame gantry has been constructed from prefabricated metal framing channel to carry the necessary equipment to pour molten aluminum. The ridge beam of the gantry spans eight feet and is at an elevation of approximately seven feet. Vertical struts extend downward from this ridge beam to carry a melt crucible mounted on an axle. Horizontal struts extend forward from the legs of the gantry and carry a frame which holds a funnel and nozzle assembly forward of, and slightly below the crucible. When melt is to be delivered, the pot axle is rotated, pouring the melt from the crucible to the funnel which delivers the melt to the test pool.

The crucibles are fabricated of type 304 stainless steel and are electrically heated. Sections of schedule 5 or 10 stainless steel pipe of appropriate diameter are cut to the required length to give the volume desired, and flat, square plates are welded on one end. Clamshell type electric resistance elements of the proper dimensions are mounted on the crucibles and typically backed up with one to three inches of ceramic fiber insulation as needed. Chromel-alumel thermocouples are spot welded on the exterior of the crucible walls to evaluate heater performance. Mounting hole locations and electrical connections are standardized, allowing fast change over of crucibles of different volumes as required for varying applications.

The funnel and nozzle assembly is also fabricated from type 304 stainless steel. It consists of a conical upper section which terminates in a flange which can be fitted with stainless steel nozzles of various diameters. The nozzle assemblies are drilled or bored to their required diameter in a lathe and are quickly interchangeable, allowing variation of the mass flow rate of melt delivered to the test tank. The funnel and nozzle assembly is also electrically heated and instrumented with chromel-alumel thermocouples to monitor funnel temperatures. The interior of the funnel is coated with high temperature ceramic cement.

The test pool is located beneath the funnel. The pool is fabricated from acrylic plastic sheet, hot gas welded into a square tank 30" w x 30" l x 24" h. The tank is mounted on a low, wheeled table equipped with screw jacks at each corner. The tank may then be rolled into position under the funnel and jacked up to the desired elevation and levelled. The tank is also equipped with discharge and return fittings that allow connection to an external electric water heater and pump assembly to provide the desired water temperature. A 3/16" thick type 304 stainless steel plate resides on the floor of the tank and protects the acrylic from damage by hot aluminum.

An electrical control package has been constructed to service this apparatus. The package provides for control of voltage and setpoint temperature for the melt crucible and funnel assembly independently of one another. Digital temperature indicators are also provided to facilitate on-the-spot observation of various component temperatures during heat-up.

Various signals are monitored during the runs using our in-house data acquisition equipment. The equipment used for this investigation consisted of a Dell 310 computer running Asyst software and using a Keithley 500A measurement system. In addition, all thermocouple signals are locally referenced to a HyCal 150°F reference junction and conditioned by a Neff filter and gain assembly at the front end of the Keithley 500A system. Specifically, the signals measured are bulk aluminum temperature in the crucible, aluminum temperature inside the funnel just above the nozzle, water pool temperature and voltage from a photocell positioned at the exit of the nozzle to give us duration of pour. A schematic representation of the experimental apparatus is presented in Figure 1.

Several other pieces of equipment are also employed to collect information from the runs. A video camera and 1/2" VHS video cassette recorder are used to record the melt entry into the water pool and subsequent activity. Measurements of jet breakup length are made in this manner. A high speed 16 mm rotating prism movie camera was used for selected runs to provide a detailed look at the jet entry morphology. Finally, a set of wire cloth testing sieves were used for a characterization of the particle size distribution.

2.2 Test Procedure

The procedure for conducting the Deep Pool aluminum tests is roughly divided into three major sections: pre-run preparations, run execution, and post-run measurements and recovery.

A number of preparatory steps are required before pouring aluminum into the deep pool test tank. A quantity of aluminum casting shot is weighed out. For these runs, the nominal mass is two kilograms. The melt crucible is filled as full as practical from the weighed mass, and as it melts down, the remaining material is added. A nozzle insert of the appropriate diameter is installed in the nozzle and funnel assembly. The funnel assembly is installed in the gantry and levelled. The deep pool test tank is wheeled under the nozzle exit and placed into a level position at the appropriate elevation. The test tank is filled to the required water depth and all the heated zones, crucible, funnel, and water are energized. As the aluminum casting shot melts down, cold casting shot is added to the crucible and stirred. The temperatures reported by the thermocouples in the aluminum are monitored during melting and compared to aluminum's known phase change temperature. In general, the values reported by the data acquisition system during the phase change are within 0.5°C of the standard value of 660.34°C. While all heated components are brought to their target temperatures, their progress is monitored by the data acquisition computer. Also during this approach to target temperature, all necessary photographic and video equipment is aligned.

When the required melt, water, and funnel temperatures are reached, non-essential personnel are cleared from the area and a secure perimeter is established and maintained during run execution. The aluminum and water are both stirred to insure uniform temperatures. The data acquisition system is switched from monitor mode to acquisition mode and is held to be started in concert with the pour. The insulating covers are removed from the crucible and funnel, the duration-of-pour light cell is activated, the video camera and lights are activated, and

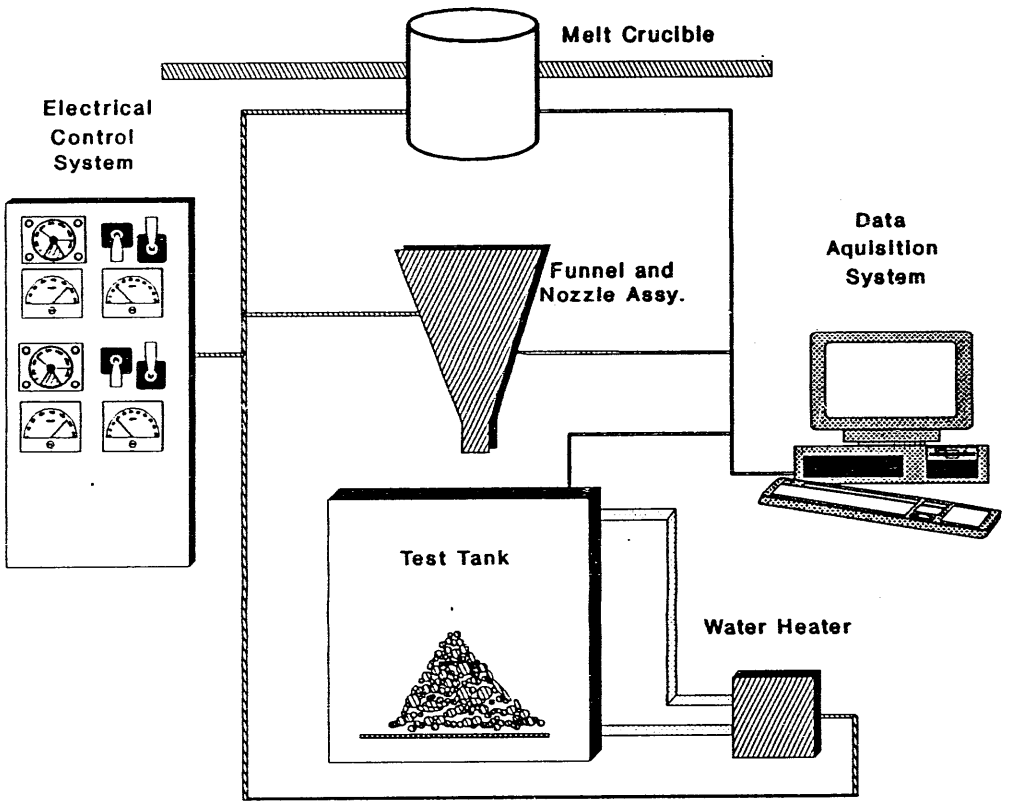

Figure 1. Schematic of Experimental Facility.

the operators assume their positions at the data acquisition computer and the crucible pouring controls. On command, the data acquisition is initiated and the aluminum is rapidly transferred to the funnel and nozzle assembly. The duration of pour is determined by the nozzle diameter and gravitational head of aluminum.

Upon completion of the run and quenching of the molten aluminum, post run recovery begins. The area is re-entered and all electrical power to the components is disconnected. The test tank is drained of its water and rolled out from under the funnel. Photographic records of the results of the test are generated. The debris, if it is particulates, is removed from the tank and dried in an oven at 240°F. The debris is then size classified by passing through a set of testing sieves, and particle density and mass fraction determinations are made. If the debris formed an ingot, its spread area is determined.

The apparent densities to be reported were obtained by a water displacement method described below. A glass cylinder, approximately 30 cm tall by 5 cm in diameter was equipped with a downward facing side arm at an elevation of 28 cm. The cylinder was clamped vertically in a ring stand and filled with water to just overflow out of the side arm. A dry graduated cylinder was then placed under the side arm, and a previously weighed, representative sample of particles was carefully submerged in the cylinder of water. The water displaced by the particles was collected in the dry graduated cylinder and represented the particle volume. The volume was then divided into the previously measured mass to give the apparent density.

Areas for the tests which resulted in spreads were measured as follows. The spread is placed on a sheet of paper, and its outline is carefully traced. The area of the tracing is then measured with a polar planimeter.

2.3 Test Parameters and Matrix

Prior to the execution of a run, there are a number of operational parameters which must be adjusted to specification. Regarding the aluminum, the target values for the runs were two kilograms at 700°C. The aluminum flow rate was varied by using nozzle diameters of either 1/8", 1/4", or 1/2". The water temperature was varied from ambient to about 70°C and its depth was varied from 25 to 50 cm. This range of conditions is considered to bound the conditions under which melting of non-fuel components in the reactor tank is likely to occur.

The actual values established for these parameters in the tests conducted are listed in Table 1.

Table 1 - Table of Test Parameters

Run	Aluminum Mass (gm)	Aluminum Temperature (°C)	Water Depth (cm)	Water Temperature (°C)	Nozzle Diameter (cm)
1	1788	703	50	23.7	0.318
2	981	690	50	42.5	0.318
3	1719	735	50	40.2	0.318
4	1391	736	50	59.0	0.318
5	1982	728	50	50.8	0.318
6	1901	718	50	22.9	0.635
7	1977	710	50	31.0	0.635
8	2059	715	50	42.0	0.635
9	1997	719	50	49.7	0.635
10	2015	720	50	60.5	0.635
11	1999	720	50	70.7	0.635
12	1938	720	25	71.9	0.635
13	1689	742	25	71.0	0.318
14	2501	666	50	53.6	1.27
15	2805	679	50	41.2	1.27
16	2570	680	30	40.0	1.27
17	2770	679	30	40.7	1.27
18	2696	684	50	40.0	1.27

3. EXPERIMENTAL TEST RESULTS

3.1 Conduct of Tests

Run #1:

Run #1 was intended to deliver nominally 2 kg of molten aluminum at 700°C into a 50 cm deep water pool at ambient temperature (~24°C) through a 1/8 inch diameter nozzle.

The test began with an unanticipated blockage in the melt delivery nozzle. The blockage was cleared by the application of heat with a torch while probing through the nozzle with a stainless steel rod. During this phase of the pour, approximately eighty melt particles were released to the pool.

Once the blockage was cleared, a coherent melt jet began to flow. During the jet phase, 1788 grams of molten aluminum were delivered over a period of 112 seconds. Finally, the termination phase of the run consisted of a period of dripping melt entry. About 100 drops of aluminum were introduced in this manner. The aluminum introduced during the dripping phases of the test was eliminated from consideration. Only the mass delivered as a coherent jet is reflected in Table 1 and all subsequent data presented.

Video records of the test indicate that the jet broke up into molten drops at some depth below the surface of the water. Jet breakup characteristics will be discussed in more detail in sections to follow. The particles appeared to freeze before landing on the floor of the tank. The frozen particles formed a conical pile of loose debris on the floor of the tank directly below the point of jet entry. Characterization of the debris will be discussed in a later section.

Run #2:

The intended initial conditions for Run #2 were identical to Run #1 except for a water temperature of 42.5°C, which represents a nominal 20°C increase over Run #1.

Again, the test began with a blockage of the nozzle assembly preventing proper delivery of the melt to the pool. Attempts were made to clear the nozzle with heat and a probe, as in Run #1. Efforts to clear the nozzle resulted in a dripping melt delivery lasting 112 seconds and delivering 981 grams of aluminum to the pool. A jet-type delivery was never established for this run.

Although the pour never developed into a jet, the particle behavior in the water pool was very similar, with the exception of jet breakup length. Review of the video tape reveals that some of the particles may be just on the verge of freezing as they land on the floor. Some of the particles appear to have become slightly attached to others as the pile on the tank floor accumulated.

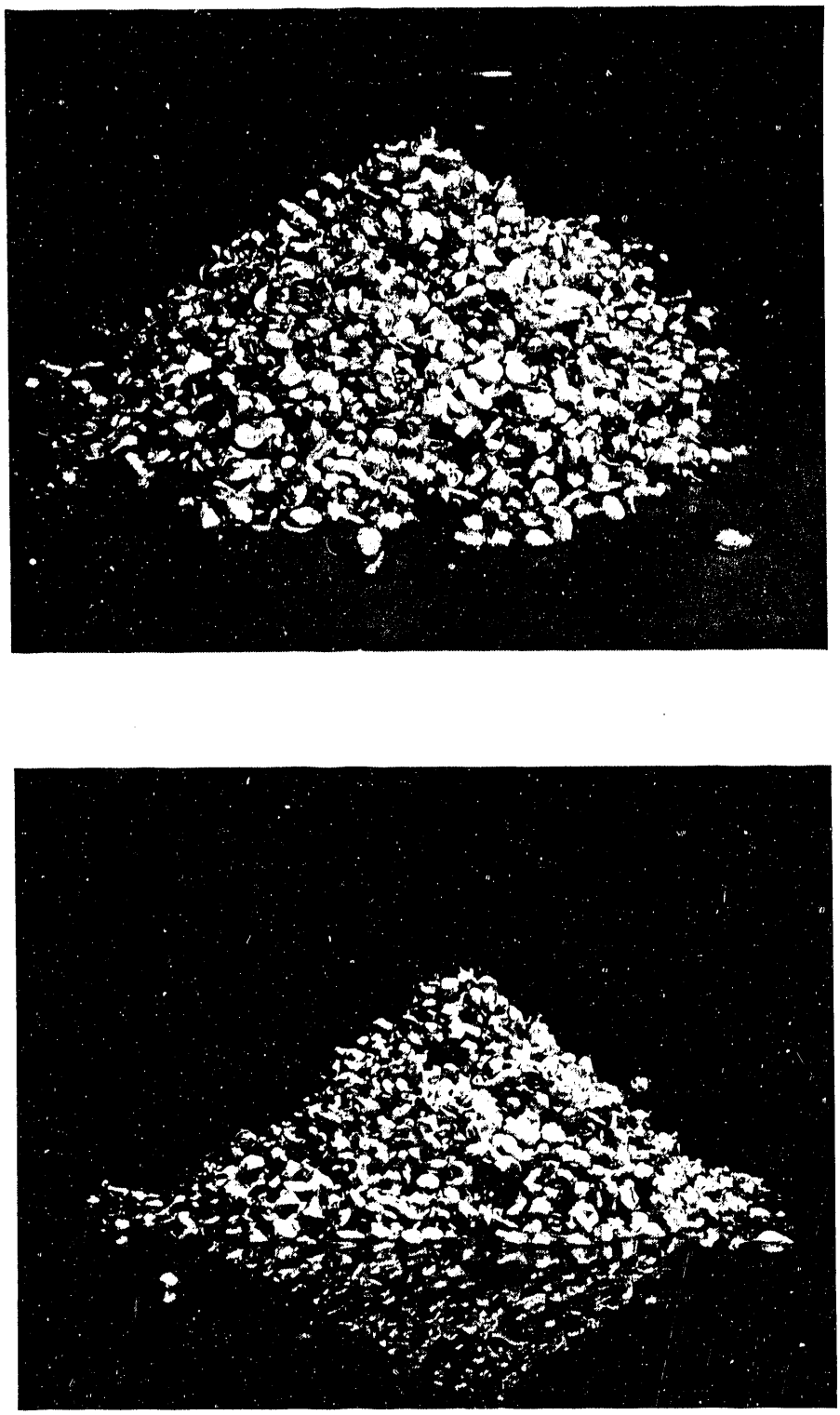

Figure 2. Morphology of Solidified Debris Resulting from Run 1.

Run #3

Run #3 was intended to duplicate Run #2, in which the jet never developed. Again, the target conditions were 2 kg of aluminum at 700°C, and 50 cm of water at 40°C.

This time, the run started cleanly, quickly forming a jet which penetrated the water surface some distance before breaking up into droplets. In the jet entry mode, 1719 grams of aluminum were delivered to the pool in 90.6 seconds. Upon completion of the jet phase, about 50 drips were introduced to the pool in about 15 seconds in a dropwise fashion, as the supply of aluminum in the funnel was exhausted. These drops were excluded from consideration.

In this run, dozens of particles were observed to be positively buoyant, i.e., they floated to the surface. Many of them appeared to rise up from near the floor of the pool and release steam at the surface of the water, ultimately falling back to the floor after cooling and possibly filling with water. The particles were also observed to stick together upon landing on the pile accumulating on the floor. Vertically oriented agglomerations were observed to form until they became unstable and fell over, allowing new ones to start. These clusters, while not strongly fused together, could be handled without breaking apart. Also, the shapes of the individual particles making up these clusters appear relatively undistorted. Approximately 20% of the delivered inventory of aluminum became tied up in these clusters.

Run #4:

The target conditions for Run #4 were 2 kg of aluminum at 700°C through a 1/8" diameter nozzle into 50 cm of water heated to 60°C. The only change compared to the previous run is the increase in water temperature of another 20°C.

Run #4 also started cleanly, quickly forming a jet which penetrated the water prior to breaking up into droplets. 1391 grams of aluminum were delivered to the pool in 94.5 seconds. Upon completion of the jet phase of the pour, only about 10 drops of aluminum entered the water in a dropwise fashion. The particles fell through the water in substantially the same manner as previous runs. Only a few particles were observed to become positively buoyant. As the particles landed on the tank floor, it became apparent that they were still molten. As droplets landed on each other, they became firmly attached and ultimately formed a pillar of aluminum about 23 cm tall and 7 to 8 cm in diameter. The individual particles making up the pillar were somewhat distorted and merged together, indicating that they were molten when they landed. About 76% of the delivered inventory was tied up in this firmly bound pillar.

Run #5

For this run, the water temperature was reduced 10°C relative to the previous run. The set of target conditions were 2 kg of aluminum at 700°C into 50 cm of water at 50°C.

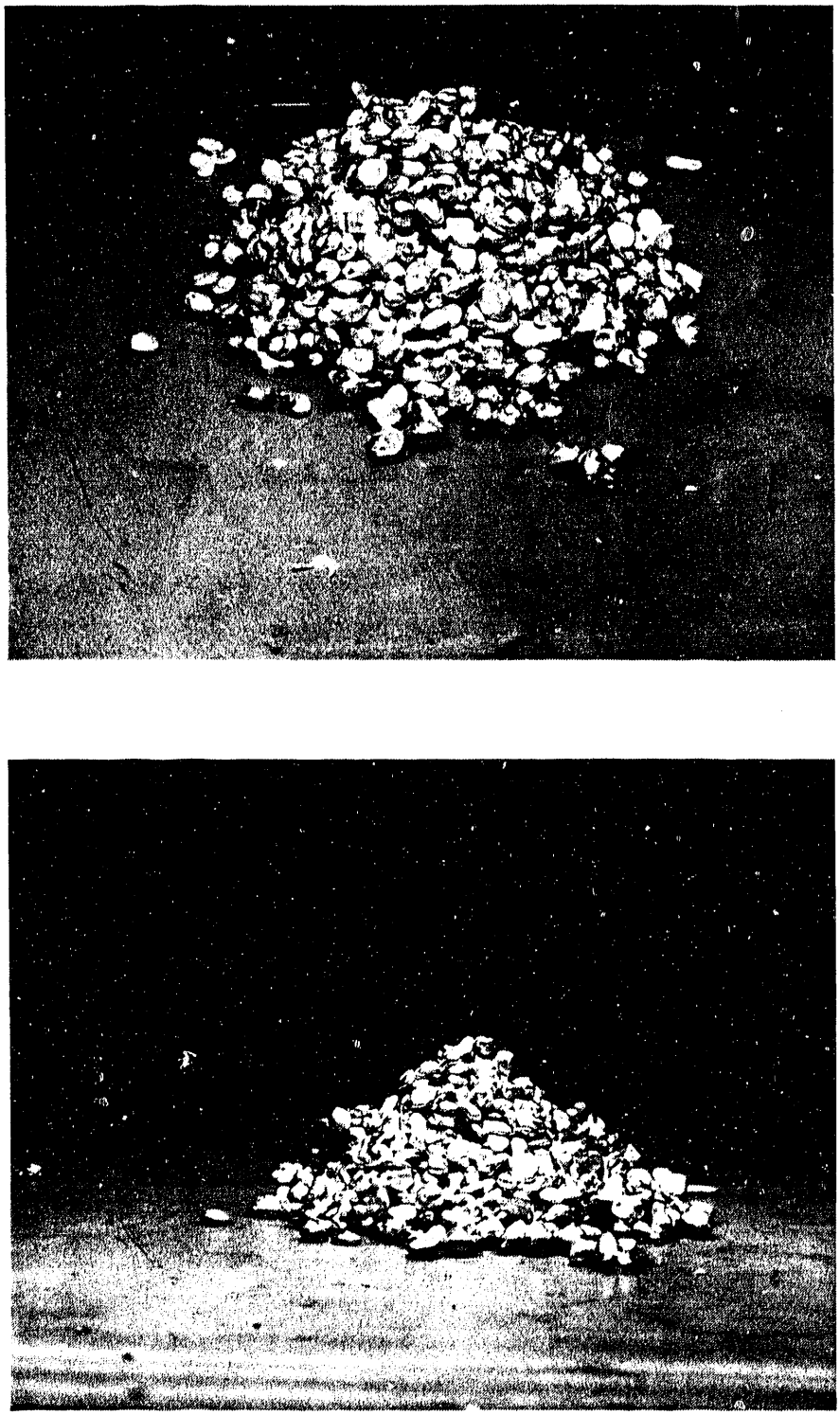

Figure 3. Morphology of Solidified Debris Resulting from Run 2.

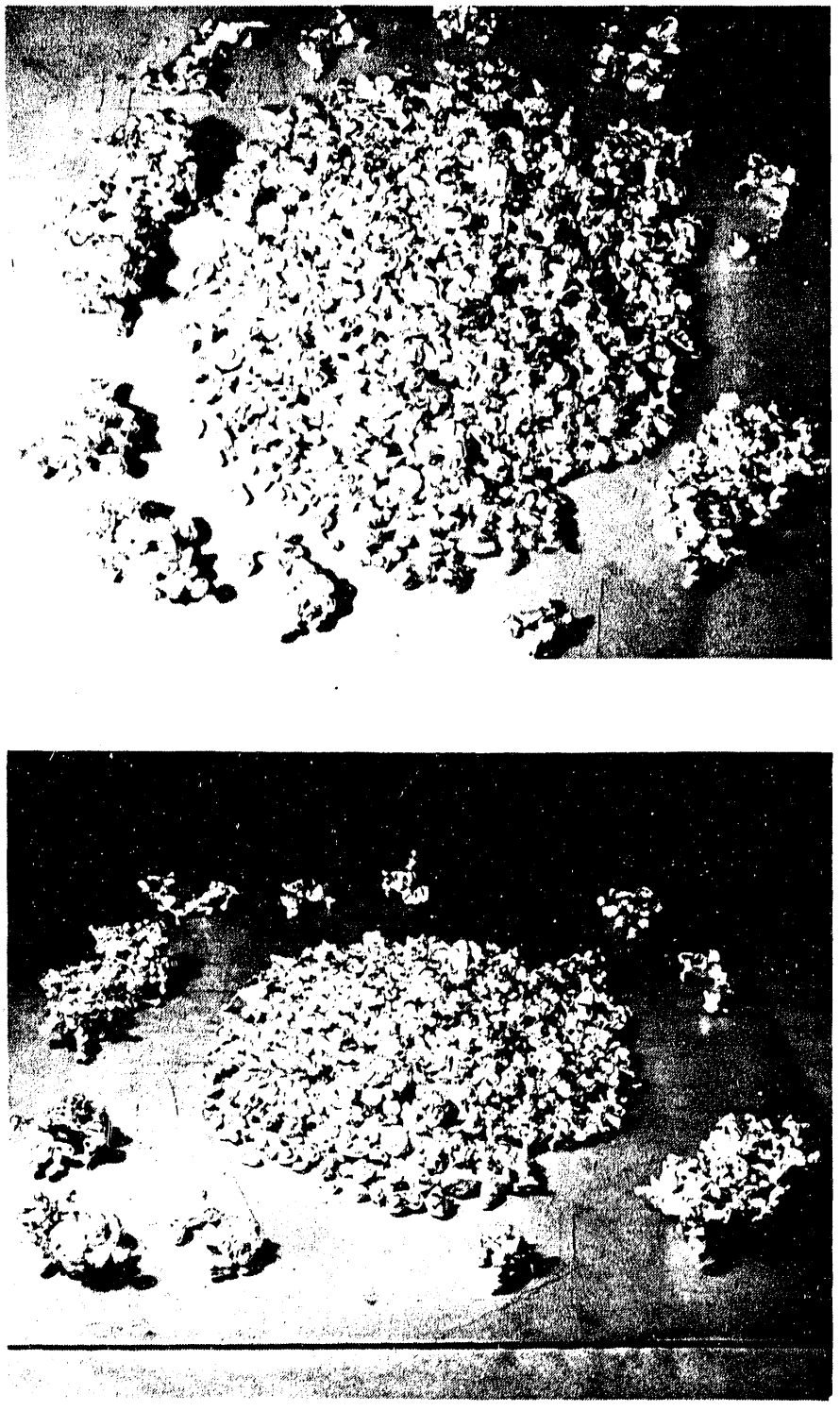

Figure 4. Morphology of Solidified Debris Resulting from Run 3.

Figure 5. Morphology of Solidified Debris Resulting from Run 4.

A structural failure of the nozzle and funnel assembly resulted in the uncontrolled introduction of aluminum to the pool. The melt entry morphology varied between periods of dropwise entry and jet like behavior, however the point of exit from the funnel was not through the 1/8" diameter nozzle, but rather through a breach in the funnel wall. A mass of 1982 grams was delivered to the pool in this manner over a period of 80.1 seconds.

The behavior of the debris in the water was similar to the previous run. A firmly attached pillar again formed, consuming about 72% of the delivered inventory in one piece. The particles making up this pillar again showed firm evidence of having been molten upon landing on the pile.

Run #6

This run was the first in the series of runs made with the 1/4" diameter nozzle. The target conditions for aluminum and water were 2 kg at 700°C, and 50 cm depth at ambient temperature (23°C), respectively.

The pour started cleanly, quickly forming a jet and penetrating the water as such. In the jet phase, 1901 grams of aluminum were delivered to the tank in 20.7 seconds. The pour ended cleanly, with only two droplets of aluminum entering the pool after completion of the jet phase.

The particle behavior in the water was analogous to other runs with low (i.e., ambient) temperature water. A loose conical pile of frozen debris accumulated directly beneath the jet entry point.

Run #7

Run #7 was conducted with the water temperature increased 10°C above Run #6, giving intended conditions as follows: 2 kg of aluminum at 700°C through a 1/4" nozzle, and 50 cm of water at 30°C.

No problems were encountered with the actual pour. Initiation was clean, progressing immediately to a coherent jet. The jet delivered 1977 grams of aluminum to the pool in 22 seconds and ended abruptly, with only one or two stray drops.

Again, after reviewing the video tape records of the run, the jet was observed to penetrate into the water some distance prior to breaking up into droplets. In this case, the particles formed a loosely attached pillar, which crumbled into several large clusters upon handling for post run inspection. About 46% of the delivered inventory was tied up in these clusters.

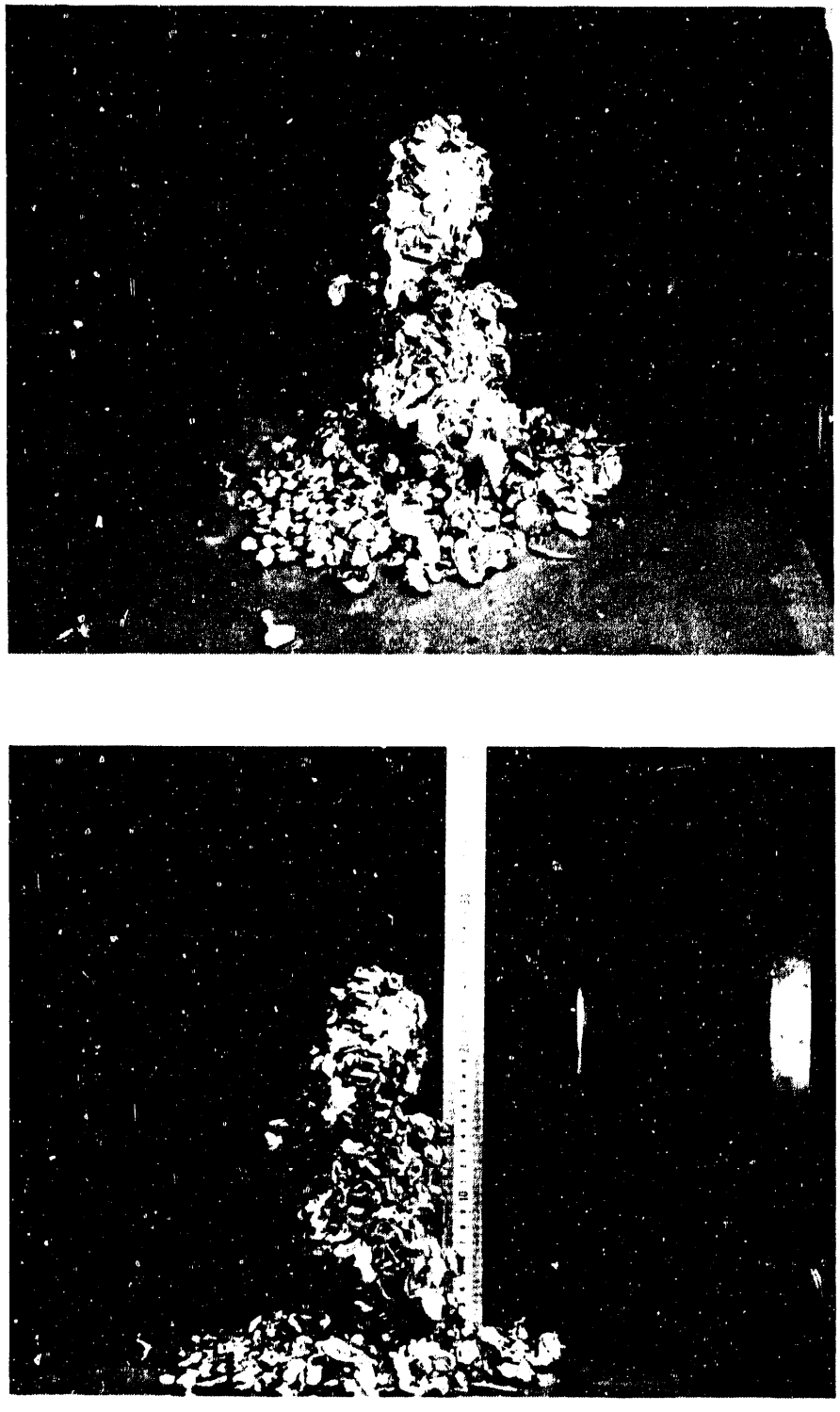

Figure 6. Morphology of Solidified Debris Resulting from Run 5.

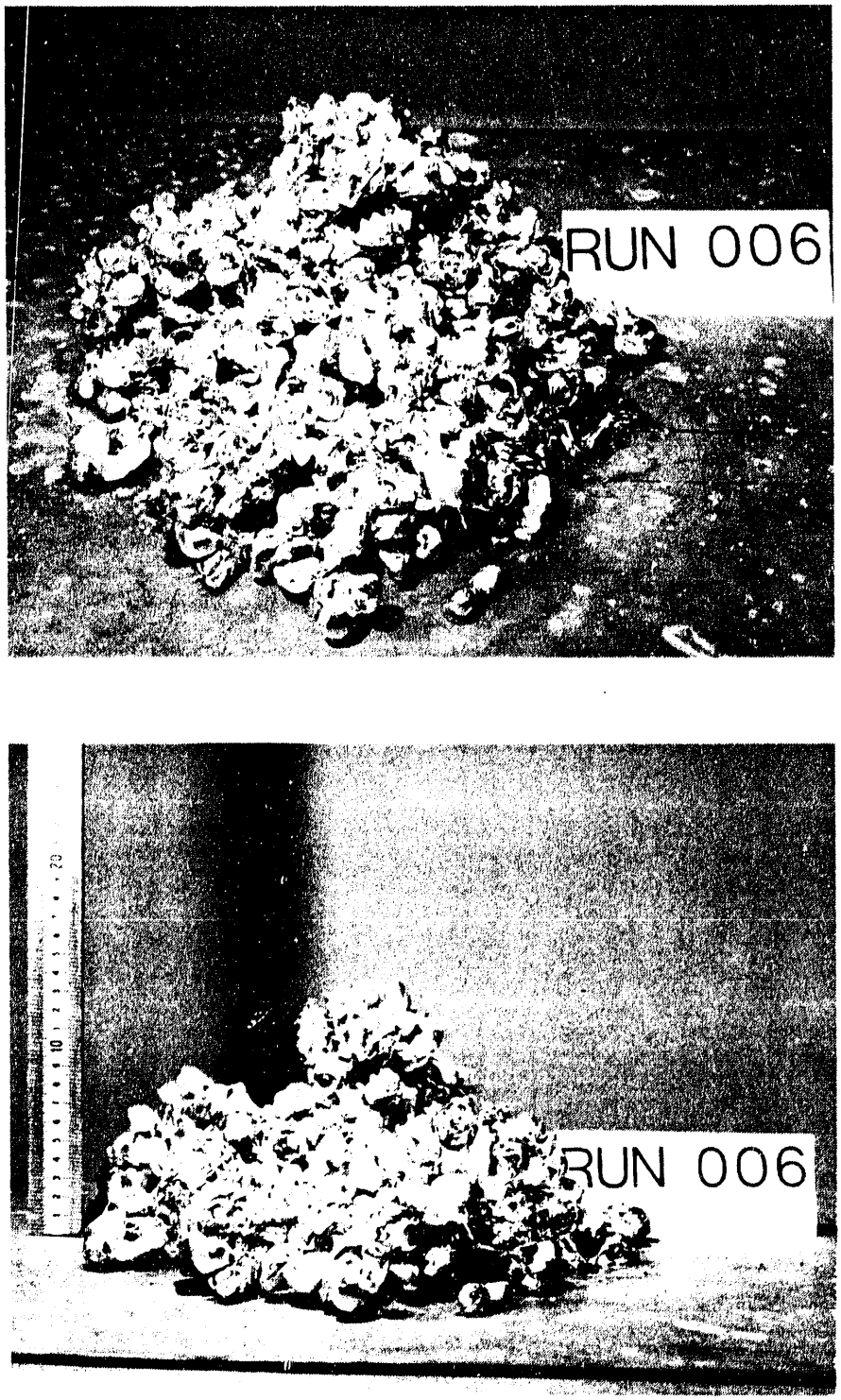

Figure 7. Morphology of Solidified Debris Resulting from Run 6.

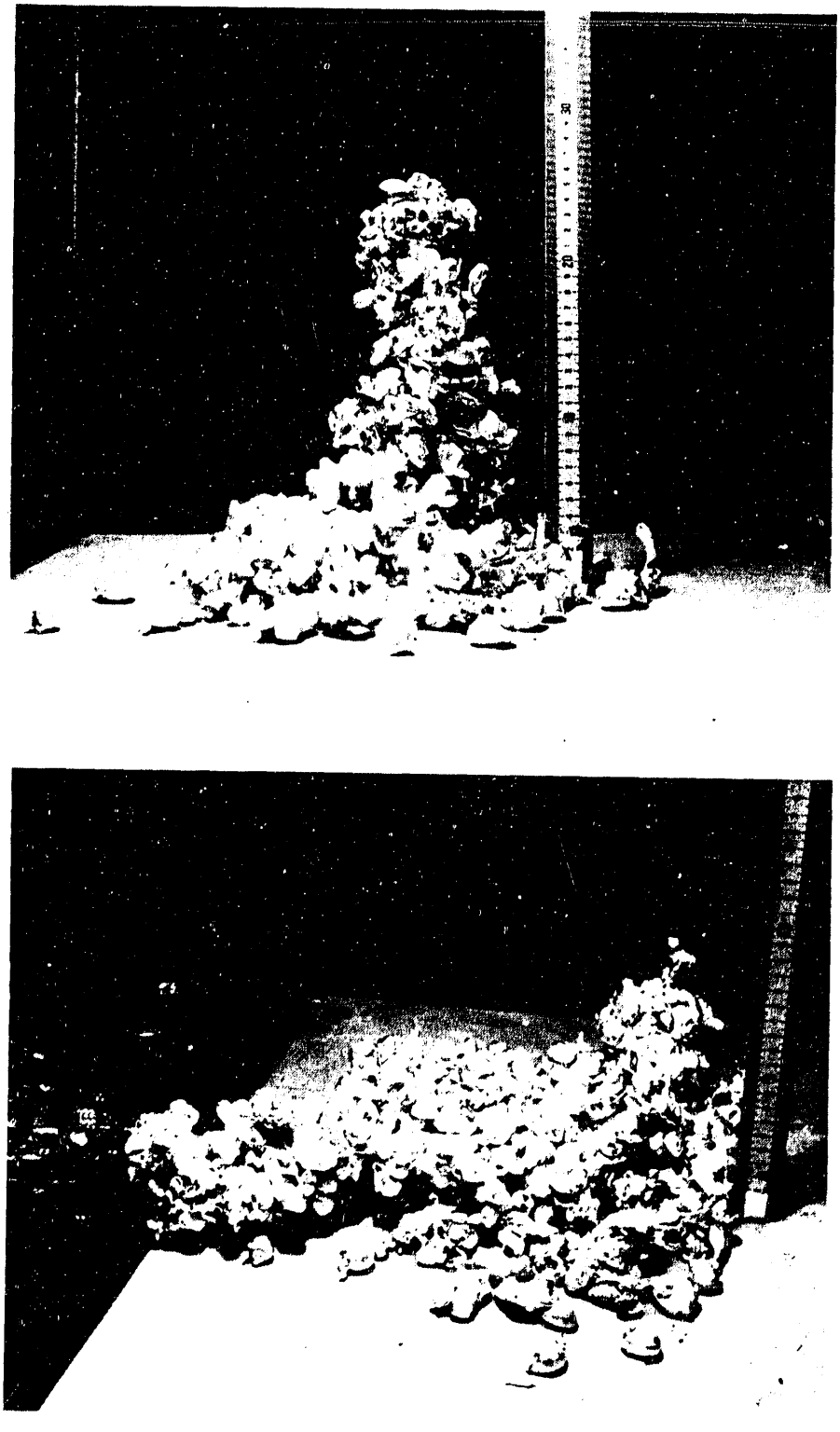

Figure 8. Morphology of Solidified Debris Resulting from Run 7.

Run #8

For this run, the water temperature was increased another 10°C, giving us intended conditions of 2 kg of aluminum at 700°C delivered through a 1/4" nozzle and 50 cm of water at 40°C.

As with other runs made with a 1/4" nozzle, there were no problems in establishing a coherent jet. The jet introduced 2059 grams of aluminum into the pool in 24 seconds. The pour ended cleanly, with no dripping melt entry.

As with previous runs, jet entry penetrated the water surface before breaking up into droplets. The droplets appeared molten during their traverse of the pool. A strong pillar of aluminum formed beneath the point of jet entry. Droplets of aluminum were observed to land on the pillar and merge with the material on top of the structure. Some aluminum was also observed to run down the sides of the pillar, analogous to wax running down the side of a candle. The pillar ultimately grew to a height of over 30 cm, and the top-most section showed no particulate character. About 82% of the delivered inventory was consumed in generating this one solid structure. About a dozen spherical particles were also observed to become positively buoyant, and float to the surface of the water pool.

Run #9

Run #9 represents another 10°C increase in the water temperature, making the intended conditions 2 kg of aluminum at 700°C into 50 cm of water at 50°C.

The pour proceeded in a manner identical to the previous 1/4" nozzle runs with respect to pour initiation , delivery and termination. A mass of 1997 grams was delivered to the pool 24.2 seconds.

Again the jet penetrated the water and broke up into droplets some distance below the surface. The behavior of the droplets as they landed on the floor, and ultimately on each other, was as in the previous run.

The pillar formed during this run, however, only reached a height of 24.5 cm, 6 cm shorter than the previous run. This pillar exhibited more coalescence than Run #8 and also more movement of aluminum as a liquid. On video tape, the structure was observed to sag and run down as material continued to fall. Some liquid aluminum was even observed slumping down the side of the pillar after the introduction of new melt had ceased.

Run #10

A further increase in water temperature for Run #10 brought us to target conditions as follows: 2 kg of aluminum at 700°C delivered through a 1/4" nozzle into 50 cm of water at 60°C.

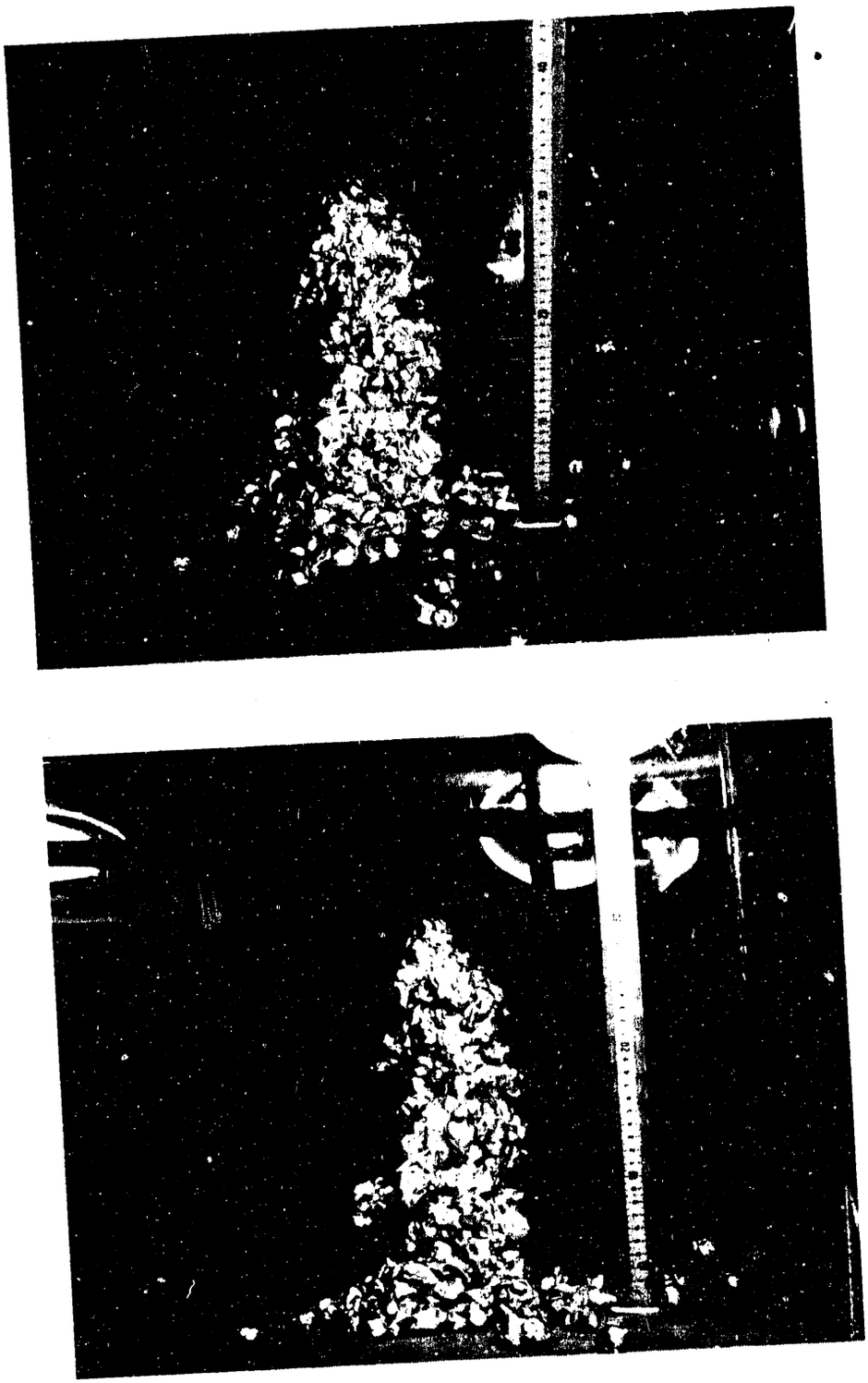

Figure 9. Morphology of Solidified Debris Resulting from Run 8.

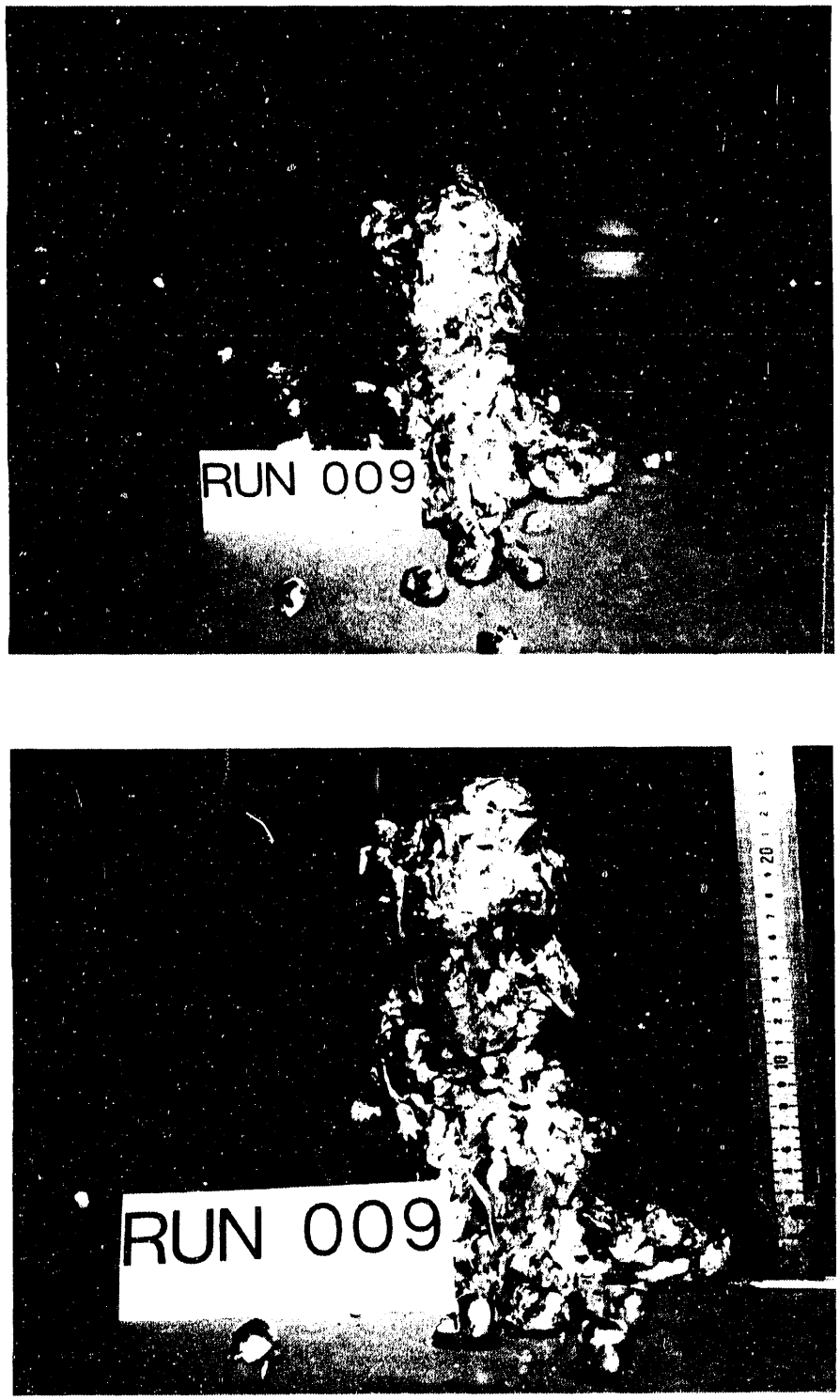

Figure 10. Morphology of Solidified Debris Resulting from Run 9.

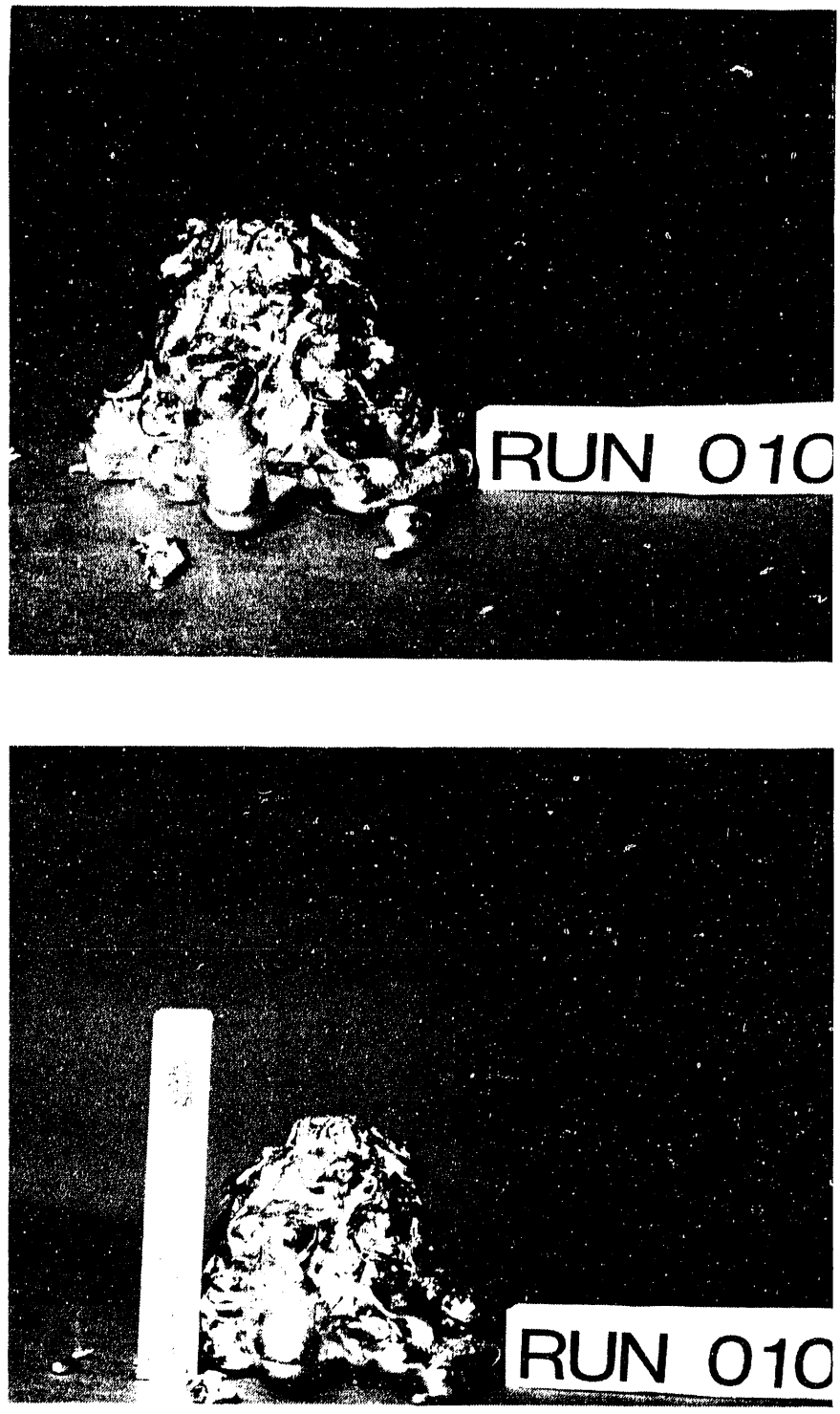

Figure 11. Morphology of Solidified Debris Resulting from Run 10.

Melt morphology was as in all previous 1/4" nozzle runs. A well defined jet was quickly established, which delivered 2015 grams of aluminum to the pool in 26 seconds. The nozzle delivered about 8 drops of molten aluminum at the end of the jet phase of melt delivery. These drops fused with the aluminum mass and could not be excluded.

The behavior of the aluminum jet in the upper and mid water regions of the pool was as in all previous 1/4" nozzle runs.

The behavior on the floor, however was somewhat different. The falling droplets coalesced into a slug of aluminum somewhat hemispherical in shape, with a height of about 12 cm and a base circle diameter of about 13 cm. The slug covered an area of 167 cm^2. The surface texture of the slug appeared irregularly sagged, and showed no trace of particulate character. Local boiling was observed on the surface of the slug. This boiling lasted about 60 seconds after the completion of the melt introduction to the pool.

Run #11

A final increase in the water temperature brought us to Run #11. The conditions intended for Run #11 were 2 kg of aluminum at 700°C delivered through a 1/4" nozzle into 50 cm of water at 70°C.

Once again, the pour resulted in rapid establishment of a coherent jet of molten aluminum which penetrated the water surface. The jet phase delivered 1999 grams of molten aluminum to the pool in 26 seconds. About 6 drops of molten aluminum immediately followed the jet phase pour.

The behavior of the melt on the floor of the tank was similar to the previous run. A slug of aluminum accumulated in a molten mass, covering 218 cm^2 of the floor area. This represented an increase in area of about 23% compared to the previous run, which had water 10°C cooler. The slug from this run had a height of about 10 cm, two cm lower than the previous run. Boiling activity was observed on the surface of the slug for about 90 seconds following completion of the pour.

Run #12

Intended conditions for Run #12 were identical to Run #11 except that the depth of the water pool was reduced to 25 cm at 70°C. The aluminum specifications remained fixed at 2 kg mass and 700°C temperature.

Some difficulty in establishing a jet was experienced during this run. Upon transfer of the melt from the crucible to the funnel, the pour began as a slow dripping pour. About 20 drops were released prior to the establishment of a well formed jet of molten aluminum. These drops were fused into the bulk of the pour and could not be excluded. The termination of the

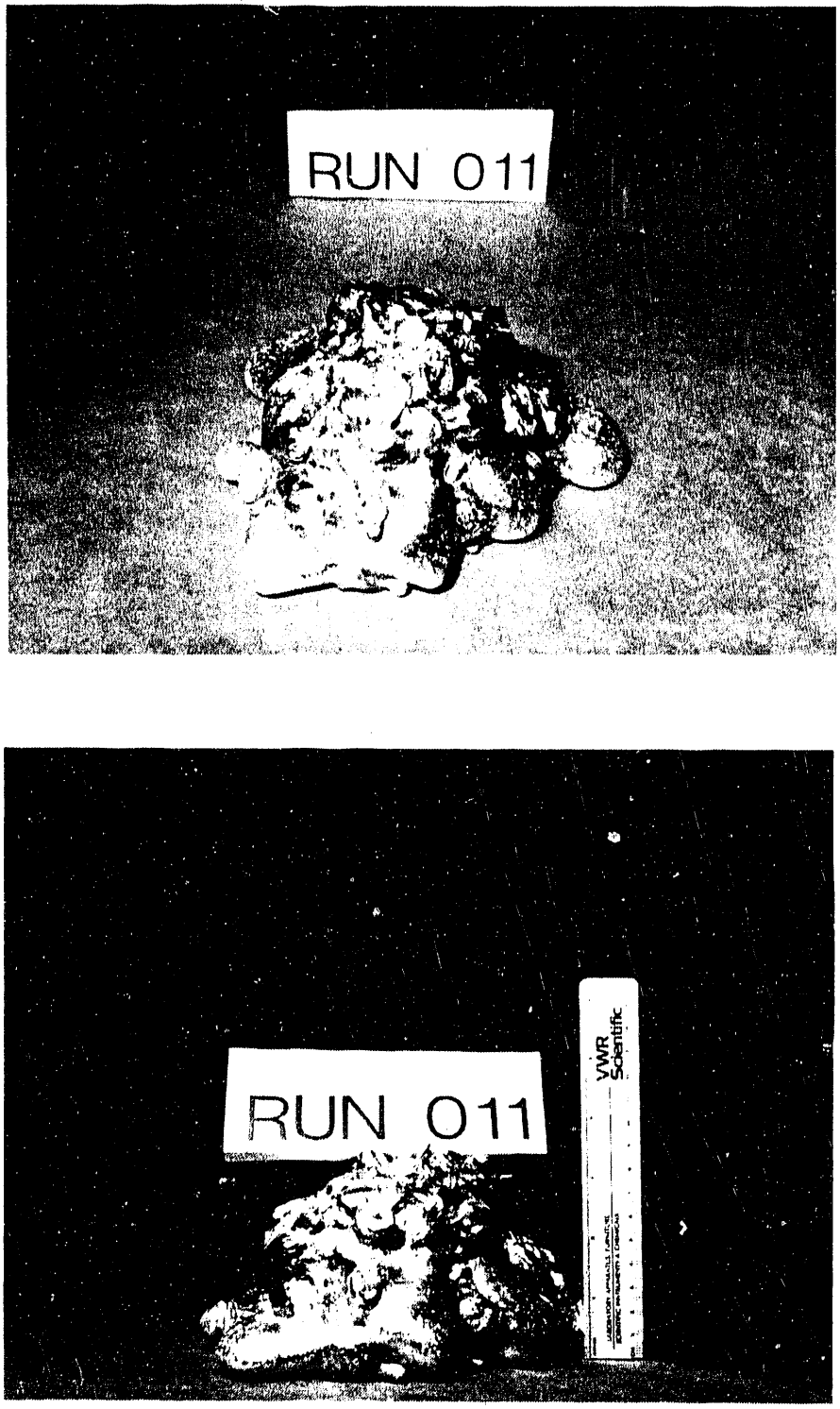

Figure 12. Morphology of Solidified Debris Resulting from Run 11.

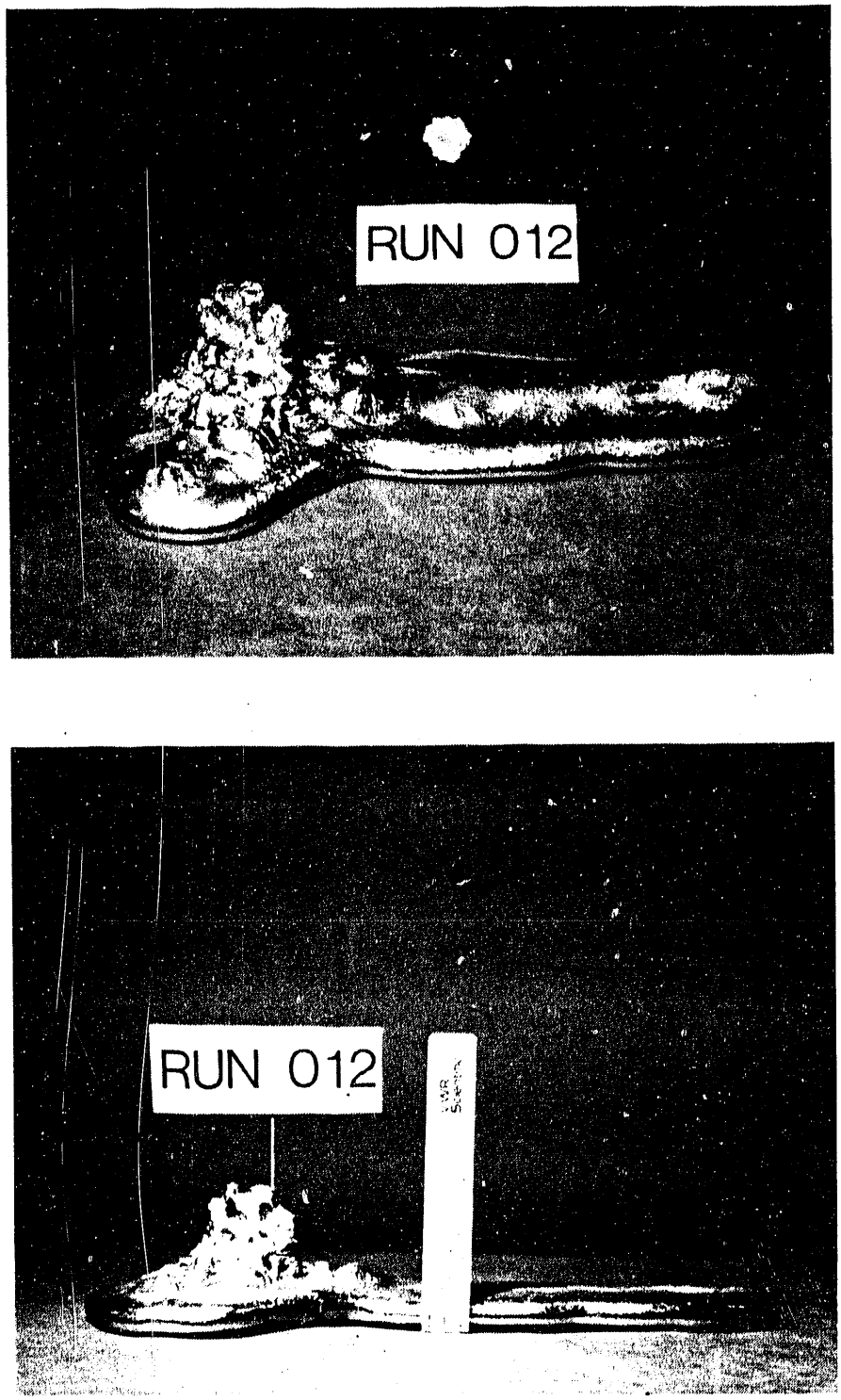

Figure 13. Morphology of Solidified Debris Resulting from Run 12.

pour was fairly clean, finishing with 4 more drops. The duration of the jet phase of the pour was 22.5 seconds.

The behavior of the jet upon entry into the water was identical to previous runs, but the behavior on the floor was somewhat different. A large proportion of the melt coalesced and spread into a flattened oblong structure covering an area of 422 cm^2. This area is almost double the area covered by the previous run, which only differed by having twice as much water. The surface texture of this spread-out structure was very smooth, as if it had been poured in the absence of water. A small slug, similar in appearance to the two previous runs was intimately attached to the flattened section and rose about 6 cm above the tank floor. The surface of the spread appeared to be in film boiling after completion of the pour. A boiling front, assumed to be the transition between film and nucleate boiling, was observed to traverse the long axis of the oblong section as the aluminum cooled. The entire duration of the observed boiling activity was about 95 seconds.

Run #13

Conditions for Run #13 were identical to Run #12 except for a change back to a 1/8" nozzle. The intended test conditions were 2 kg of aluminum at 700°C through a 1/8" nozzle into 25 cm of water at 70°C.

In a manner similar to the other 1/8" diameter nozzle tests, some minor difficulty was experienced in establishing a jet. The pour began as a series of drops, until mechanical agitation with a probe in the vicinity of the nozzle opening caused the aluminum to begin to flow properly. The pour then proceeded in the usual manner, ending with several drops falling singly after completion of the jet phase. From observation of the video tape, an estimate of the number of drops introduced to the pool before and after the jet phase was made. An estimate of the mass associated with these drops was made based on the mass of particles typically produced by dripping through a 1/8" diameter nozzle. The mass of the pour was corrected by this amount. During the jet phase of the pour, 1689 grams of aluminum were delivered to the pool in 81 seconds.

The behavior of the melt in the water was similar to the previous run in surface characteristics, but was smaller in area by a factor of 2.7 and taller by a factor of about two. Much of the aluminum was observed to be molten and relocating itself in the slug that formed. Upon completion of the run, boiling behavior similar to the previous run was again observed.

The debris that resulted from each of the thirteen tests just discussed is shown in Figures 2-14.

Runs #14-18

These five runs were performed only to augment the data base for jet breakup length. An average of 2.7 kg of melt was delivered through a 0.5 inch diameter nozzle into a deep water

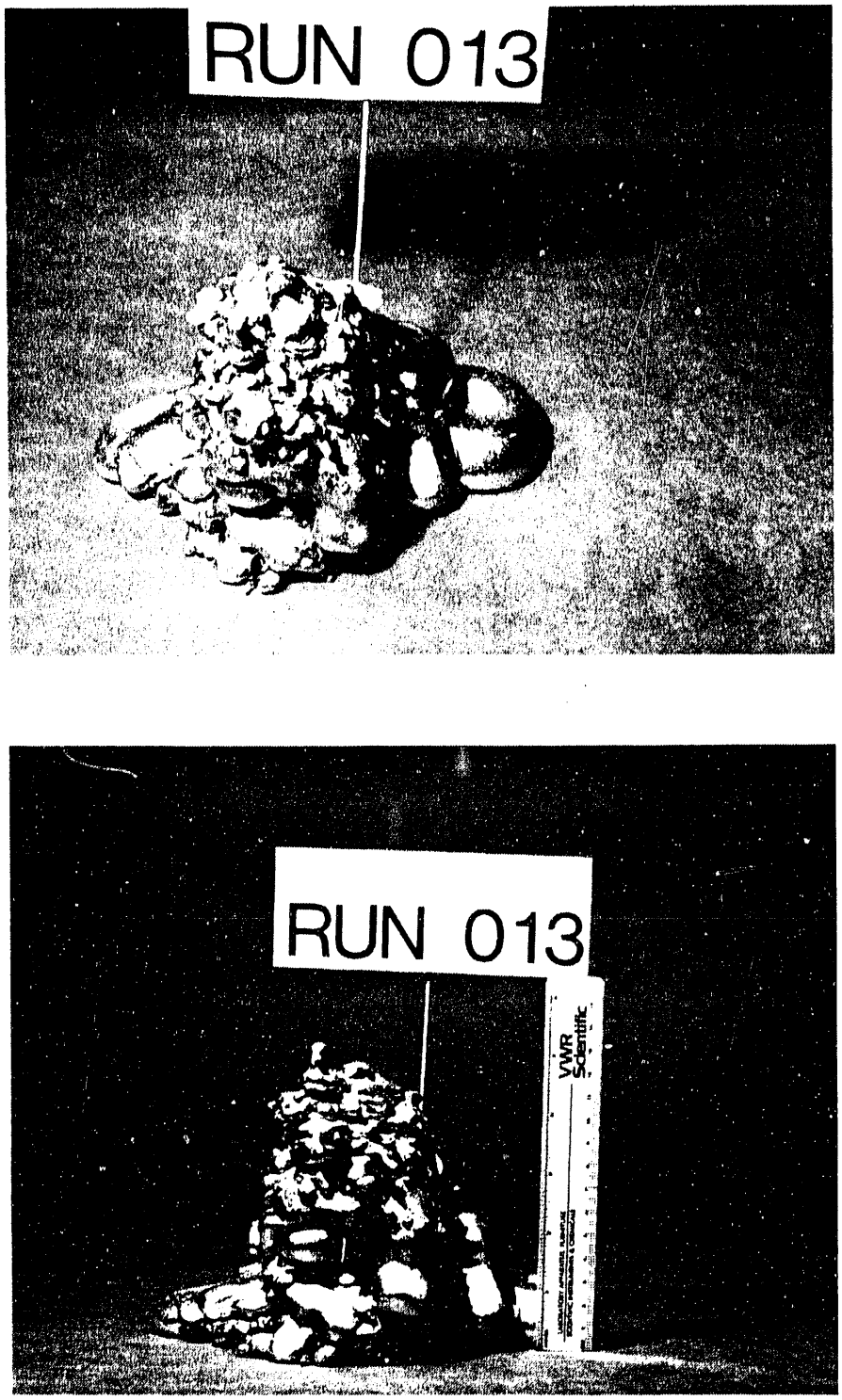

Figure 14. Morphology of Solidified Debris Resulting from Run 13.

pool (30-50 cm deep) at an average temperature (for the five tests) of 43° C. No observations other than jet breakup length were made for these tests. The performance of these tests was identical to that of the 0.25 inch nozzle tests previously described. The jet breakup lengths are recorded in Table 2 and will be discussed, along with the other jet breakup data, in Section 3.2 of this report.

3.2 Molten Aluminum Jet Breakup Length

In order to assess the potential impact of gamma heating during a DEGB-LOCA, it is useful to make quantitative measurements of the molten aluminum jet behavior as it penetrates through a water pool. The phenomena of most interest are the jet breakup length, debris size distribution, debris density, and melt spreading behavior. In this section, we will discuss measurements of the jet breakup length.

A total of eighteen tests were performed in this study of gamma heating effects. However, two of the tests involved a dripping mode of melt entry into the water pool due to the accidental formation of a blockage in the nozzle. Therefore, only sixteen of the tests resulted in jet entry and these will be discussed in this section.

In the performance of these tests, circular nozzles of 0.125, 0.250 and 0.500 inch diameters were used to direct the flow of molten aluminum downward into the water pool as a jet. A nominal mass of two kilograms of molten aluminum was heated in the melt crucible and remotely transferred to the heated funnel at a controlled rate. The melt flowed through the nozzle which functioned as both a flow straightener and to establish the initial jet diameter; the jet then accelerated under gravity to the pool surface. Water pools used in these tests varied in temperature from 23°C to 72°C. The time-averaged mass flow rate was calculated from the time-of-flight signal from the light cell device located at the exit of the nozzle. The melt density and nozzle diameter were then used to infer the average jet velocity at the nozzle exit. The initial jet velocity and diameter were corrected for acceleration effects from the nozzle to the water pool surface; it is these corrected values that are used in the data analysis, specifically in the jet Weber number and the dimensionless jet breakup length.

A classical dimensionless representation of jet breakup data due to Taylor (1942) presents the dimensionless jet breakup length, L^*, versus the jet Weber number, We. These variables are defined as,

$$L^* = (L/d_j)\ (\rho_c/\rho_j)^{0.5} \tag{1}$$

and

$$We = (\rho_j\ d_j\ u_j^2)/\sigma \tag{2}$$

For Weber numbers greater than 1000, Taylor's analysis predicted that the jet breakup length is a constant, independent of the Weber number, equal to five. For Weber numbers less than 1000, Marshall et al. (1988) correlated some breakup data in the literature and found the following empirical relationship to correlate the data quite well:

$$L^* = 200\ We^{-0.6} \tag{3}$$

Note that L^* decreases with increasing Weber number until intersecting the high Weber number asymptote of five, from whence L^* is a constant.

The data from the present experiments are listed in Table 2 and shown graphically in Figure 15 along with the IJET data of Marshall, et al (1988). A considerable base of data was used by Marshall in developing the low Weber number correlation; this data has been omitted from the figure for simplicity; only the data from the present study is shown. The data and citations may be readily accessed from the paper of Marshall, et al. (1988). It is remarkable that not only do the IJET data agree well with Taylor's model (1942) ($L^* = 5$), but that the present data agree quite well with Marshall's correlation as well (shown in the figure as the sloping line). A significant gap exists in the data over the Weber number range of 200 to 2000. Future tests are planned to fill in this gap, if there aren't already data in the literature to do so.

It is apparent that the breakup length of small diameter jets can be predicted quite well. These data and models predict that small diameter jets that could be expected under gamma heating conditions would break up into melt droplets within 20 to 40 jet diameters after penetration of the water pool. This distance (10-20 cm) is shorter than the depth of water expected to remain in the bottom of the reactor tank (25-50 cm), indicating a strong possibility of debris bed formation.

3.3 Debris Size Characterization

The characterization of the debris resulting from the deep pool tests required the use of several pieces of equipment. For runs resulting in particulate debris, a set of eight inch diameter testing sieves was used to classify the debris by particle size. The sieves provided mesh openings as follows: 1", 0.75", 0.5", 0.132", and 0.0937". The mass of all sieved fractions were determined by using a Mettler 3862MP8-1 electronic balance. Debris which was not particulate in nature was characterized by physical measurements with various rulers, gauges, and calipers.

A standardized procedure was developed for the treatment of particulate debris. After photographs of the results of the run were taken, the particles were removed from the tank and transferred to a strainer. After the water was allowed to drain, the particles were placed in an oven at 240°F overnight to remove any water trapped in particle structure. After cooling to ambient temperature, the particles were weighed to determine total mass delivered to the pool. Next, the sieves, stacked in order of decreasing mesh opening from top to bottom, were loaded with a quantity of debris from the run. The sieve stack was shaken to facilitate separation of

Table 2 - Jet Breakup Data

Run	u_j (cm/s)	d_j (cm)	L (cm)	$\frac{L}{d_j}$	We	L^*
1	211.1	0.20	7.6	37.6	24.4	24.48
3	218.1	0.22	8.0	36.9	28.0	24.03
4	209.4	0.20	8.0	40.4	23.5	26.32
6	228.8	0.47	13.0	27.9	66.1	18.18
7	227.5	0.46	13.0	28.1	64.9	18.31
8	224.2	0.45	11.0	24.3	61.8	15.81
9	222.5	0.45	12.0	26.8	60.1	17.44
10	219.4	0.44	12.0	27.4	57.2	17.83
11	214.9	0.42	11.0	26.1	52.8	16.99
12	312.4	0.39	12.0	31.1	102.1	20.25
13	311.1	0.19	6.0	31.5	50.0	20.51
14	225.5	0.84	17.0	20.3	115.8	13.2
15	271.1	0.86	20.0	23.2	172.0	15.1
16	310.6	0.84	19.0	22.7	218.6	14.8
17	289.6	0.83	18.0	21.7	188.8	14.1
18	301.9	0.78	17.0	21.9	191.9	14.3

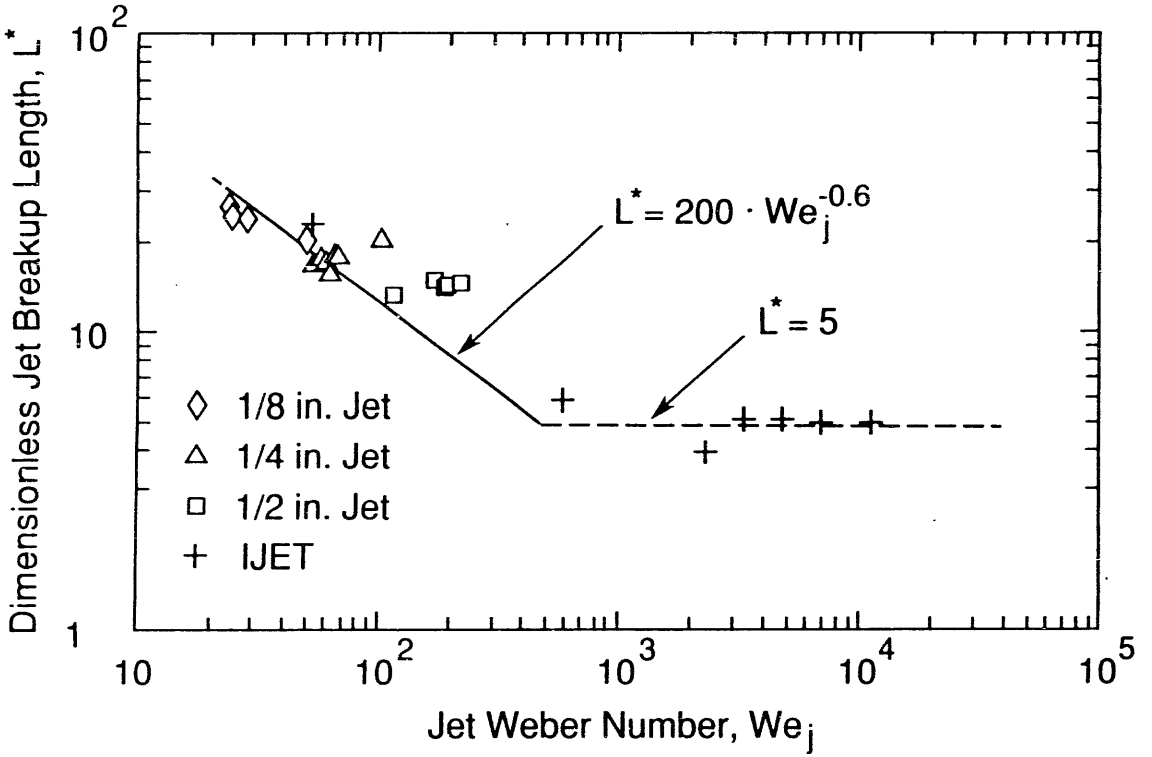

Figure 15. Dimensionless Jet Breakup Length.

the batch of particles introduced. When it was observed that there was no further relocation of material down the sieve stack, the fractions were removed to separate containers. This process was repeated with successive batches of particles from the run under test until all particles of that run were classified. Finally, each size fraction was weighed individually to allow computation of the associated mass fraction.

The debris size and shape, over the range of water temperatures and aluminum flow rates studied, showed wide variation. Debris size varied from less than 0.0937 inches in diameter to single 2 kg slugs. It should be noted, however, that the mass fraction of debris below 0.13 inches in diameter never exceeded 0.007 and in most of the runs was 0.001 or less.

Several different shapes were observed in the debris. In the 0.13-0.5 inch fractions, flattened pellets were found, as well as spherical shapes. Some elongated dumbbell shaped particles were also seen. Numerous particles with spherical shapes appeared to be hollow to varying degrees. Debris in the 0.5 - 0.75 inch fraction had a similar appearance, only with fewer pellet like particles and more hollow spherical structure. In the 0.75 to 1 inch fraction, we found irregular agglomerations of smaller particles and also some large hollow spherical structure. The fraction greater than 1 inch typically consisted of large agglomerations of smaller particles, very irregular in shape, and a few large hollow spherical structures. The mass associated with towers or slugs formed at the higher water temperatures is also included in this fraction.

The temperature of the water pool had a significant effect on particle size distribution. Increasing water temperature shifted the predominant particle size towards larger particles. For the case of the 0.125 inch nozzle, ambient temperature water (nominally 20°C) produced a distribution with almost 90% of the mass in the 0.13 to 0.5 inch fraction. As the water temperature was increased to 70°C, the mass in this fraction decreased to 2.8%. During this decrease, the mass in the fraction greater than 1 inch increased from 0% to over 96%. The intermediate fractions were at their maximums at water temperature equal to 40°C. At water temperatures above 40°C these fractions decrease to near zero at 70°C. For the 0.250 inch nozzle, with its mass flow rate of aluminum higher by a factor of four, the trends are the same, but the actual size distribution is different. The mass carried by the 0.13-0.5 inch fraction is at a maximum of 3% at near ambient water temperature and falls to 0% at 60°C. At 20°C water temperature, the distribution of mass in the three larger size classes is virtually equal. As water temperature increases, the intermediate size fractions decrease to zero while the fraction greater than 1 inch increases to 100% at 60°C water temperature.

By comparing runs with different nozzle sizes but similar water temperatures, we can get an idea of the effect of flow rate of aluminum on the particle size distribution. At ambient water temperature (around 20°C) the 0.125 inch nozzle run has 89% of its mass in the 0.13 to 0.5 inch fraction while the 0.250 inch nozzle run has only about 2% in that fraction. The balance of its mass is distributed in the larger fractions. At a water temperature of 40°C the 0.125 inch nozzle run is more equally distributed among the various size classes, but still carries 44% of its mass in the 0.13 to 0.5 inch size. The distribution in the 0.250 inch nozzle run is already

shifted to 87% of its mass greater than 1 inch. At 60°C water temperature, the 0.125 inch nozzle run has 76% of its mass in the largest size class, but is still carrying 15% of its mass in the 0.13 to 0.5 inch size class. The 0.250 inch nozzle, however, has all of its mass tied up in one slug with a mass of 2018 grams. These trends suggest that an increase in the mass flow rate results in a shift towards larger particle sizes.

Bar charts which show particle size distributions for the different tests are displayed in Figure 16 for all the runs and in Figures 17-19 for three categories of runs (1/8 inch jet, 1/4 inch jet, free drip pours) versus water pool temperature.

3.4 Debris Density Characterization

The procedure used to measure the particle densities has been outlined in Section 2.2. Briefly, the particle densities were measured by a water displacement method for all size classes where the measurements were practical.

The average particle densities were observed to vary from a low of 0.909 gm/cm^3 to the bulk density of aluminum at 293 K, of 2.7 gm/cm^3. Some individual particles exhibited densities as low as 0.6 gm/cm^3. Apparent particle density data vs. water temperature for each particle size class are presented in Figures 20-23.

For the size class 0.132 to 0.5 inch, no clear trend in the relationship between aluminum density and pool water temperature can be seen for either the 0.125 inch or 0.250 inch nozzle runs. It is apparent, however, that these densities never approach the bulk density of aluminum, indicating some degree of porosity in the structure of the particles. The two middle particle size classes, 0.5 to 0.75 inch and 0.75 to 1 inch, suggest a trend towards an increase in density with increasing water temperature for the 0.125 inch nozzle tests, but that trend is not suggested by the 0.250 inch nozzle data. The densities shown in Figure 23 for particles larger than 1 inch in diameter do not include densities of large tower or slug structures formed. The 0.250 inch nozzle data suggests a minimum of about 1.4 gm/cm^3 in the 30°C to 40°C water temperature range.

The 0.125 inch nozzle runs did not produce particles in this size class except at a water temperature of 50°C, where the particle density was slightly over 2.0 gm/cm^3 but still below the 2.7 gm/cm^3 solid phase aluminum bulk density. Figure 24 illustrates the overall average particle densities for each run vs. water temperature. The 0.125 inch nozzle data again shows no trend, but variation between about 1.7 to 2.1 gm/cm^3 over the range of water temperature from 20°C to 60°C. The 0.250 inch nozzle data is always slightly lower than the comparable 0.125 inch nozzle data and suggests a minimum in the 30°C to 40°C water temperature range, of 1.35 gm/cm^3. At 60°C the 0.250 nozzle run had formed a single slug with approximately the bulk aluminum density.

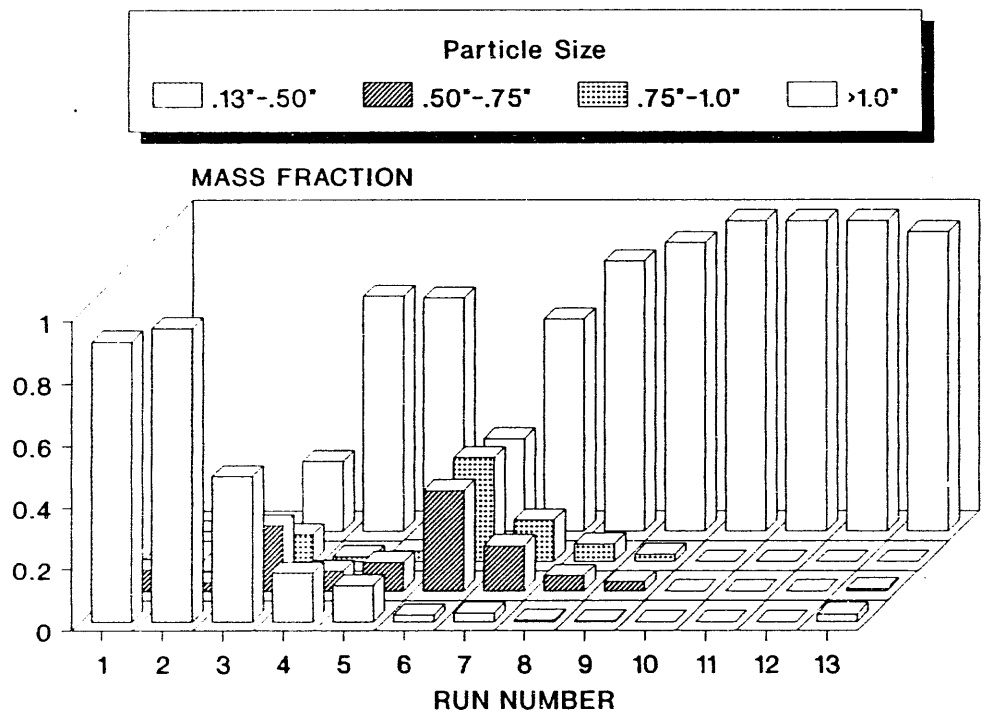

Figure 16. Particle Size Distributions for Runs 1-13.

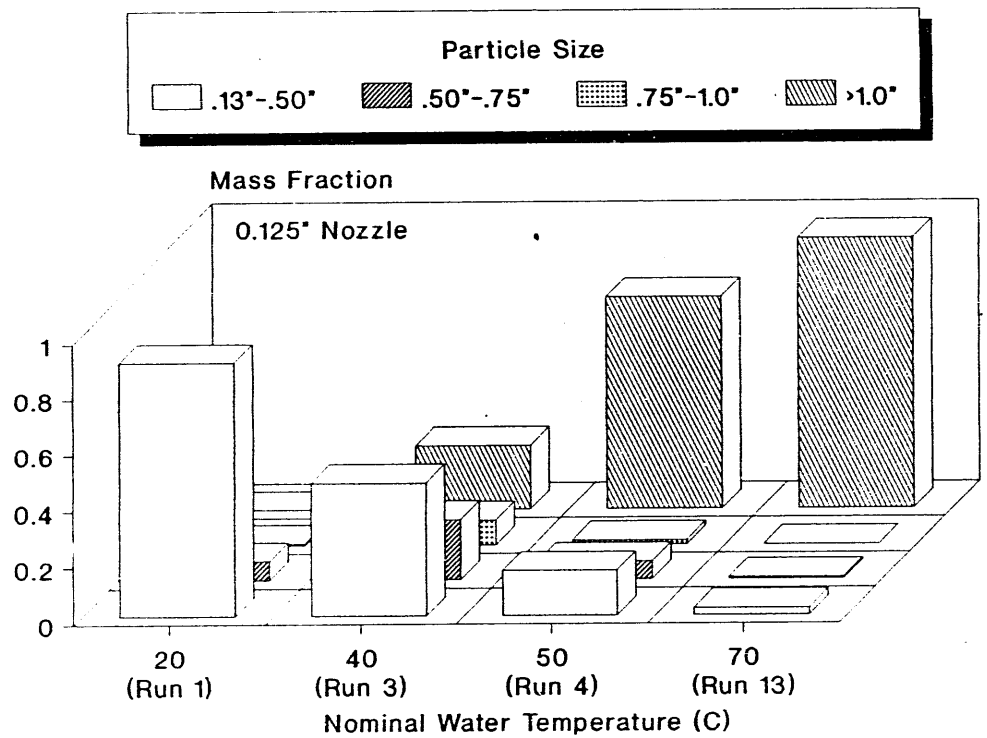

Figure 17. Particle Size Distributions for Runs 1,3,4,13.

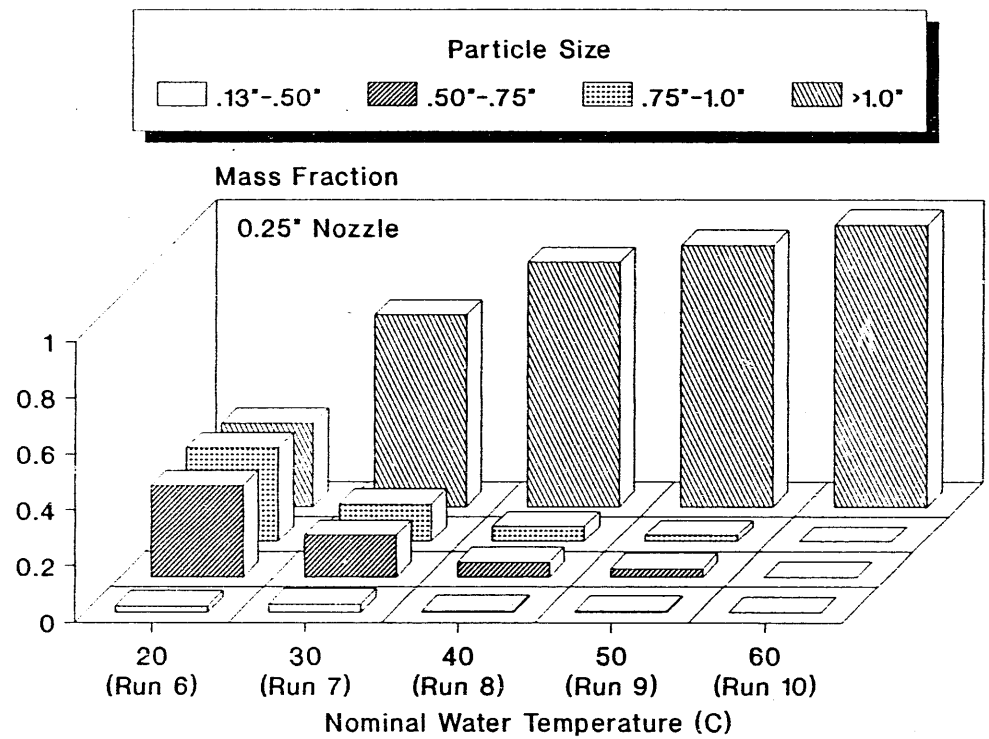

Figure 18. Particle Size Distributions for Runs 6,7,8,9,10.

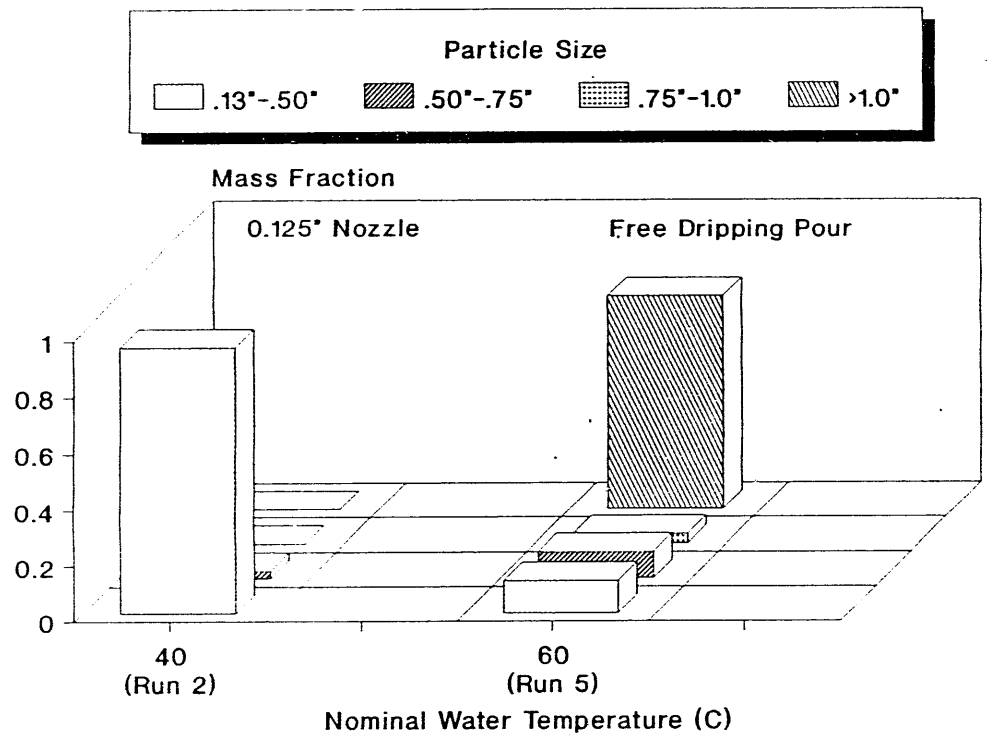

Figure 19. Particle Size Distributions for Runs 2,5.

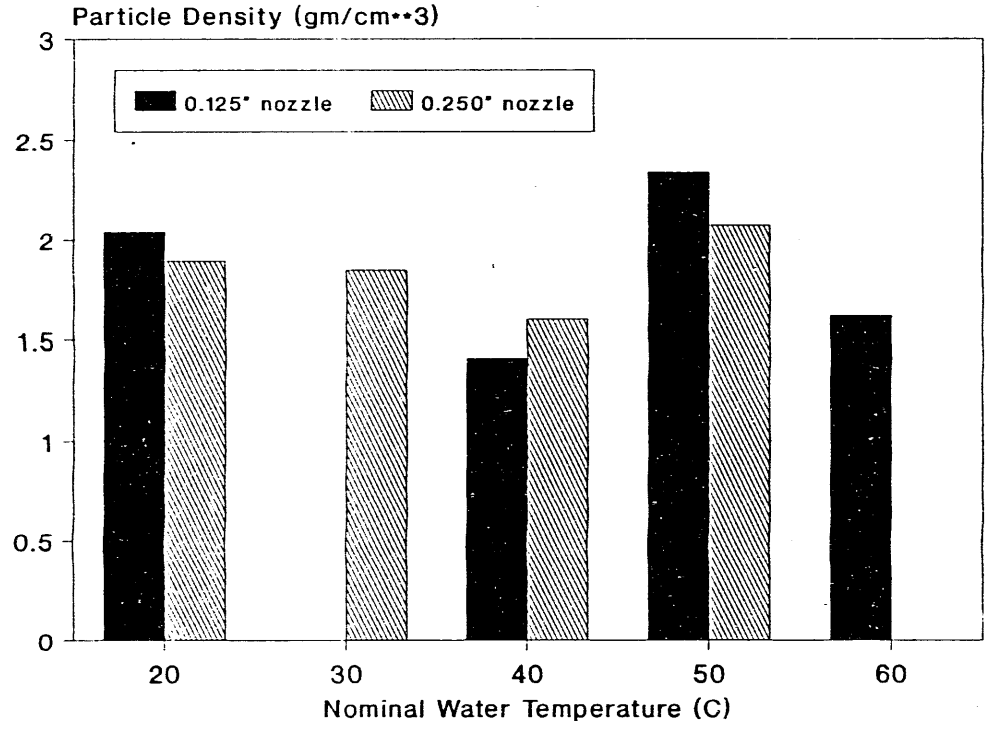

Figure 20. Particle Density vs. Water Temperature for Particles in the Range 0.132 - 0.5 inch.

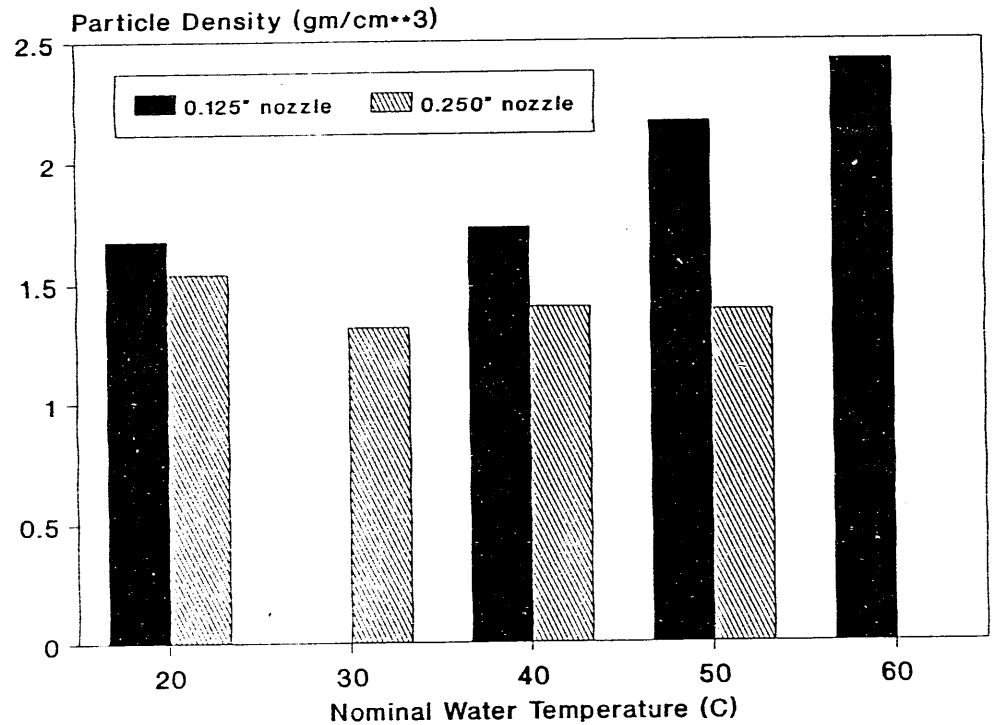

Figure 21. Particle Density vs. Water Temperature for Particles in the Range 0.5 - 0.75 inch.

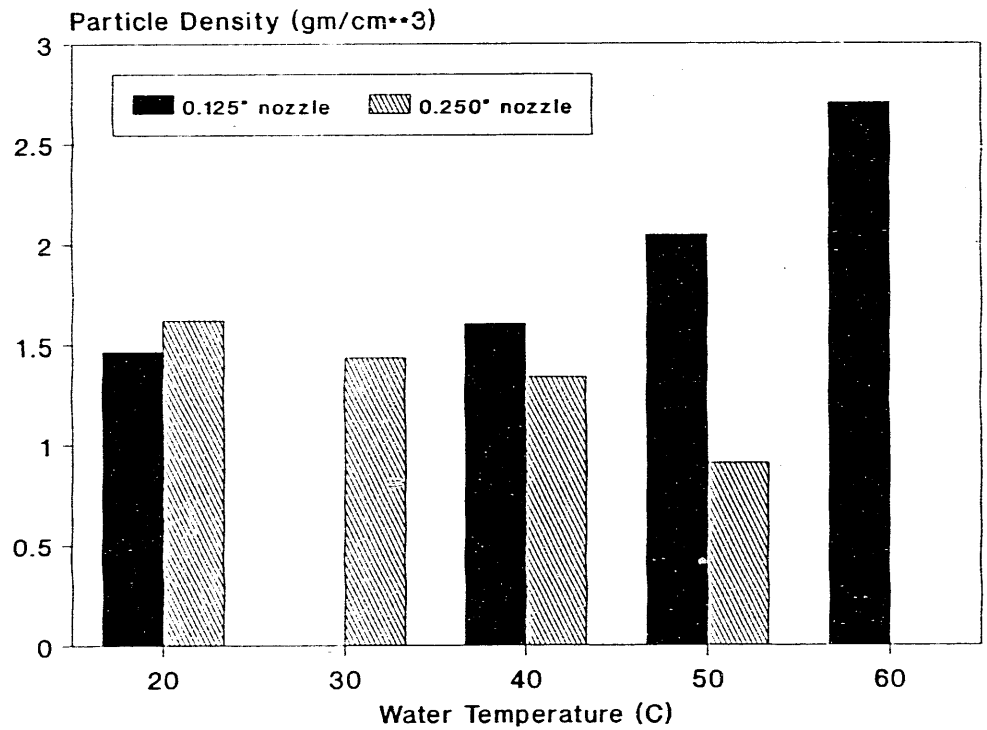

Figure 22. Particle Density vs. Water Temperature for Particles in the Range 0.75 - 1.0 inch.

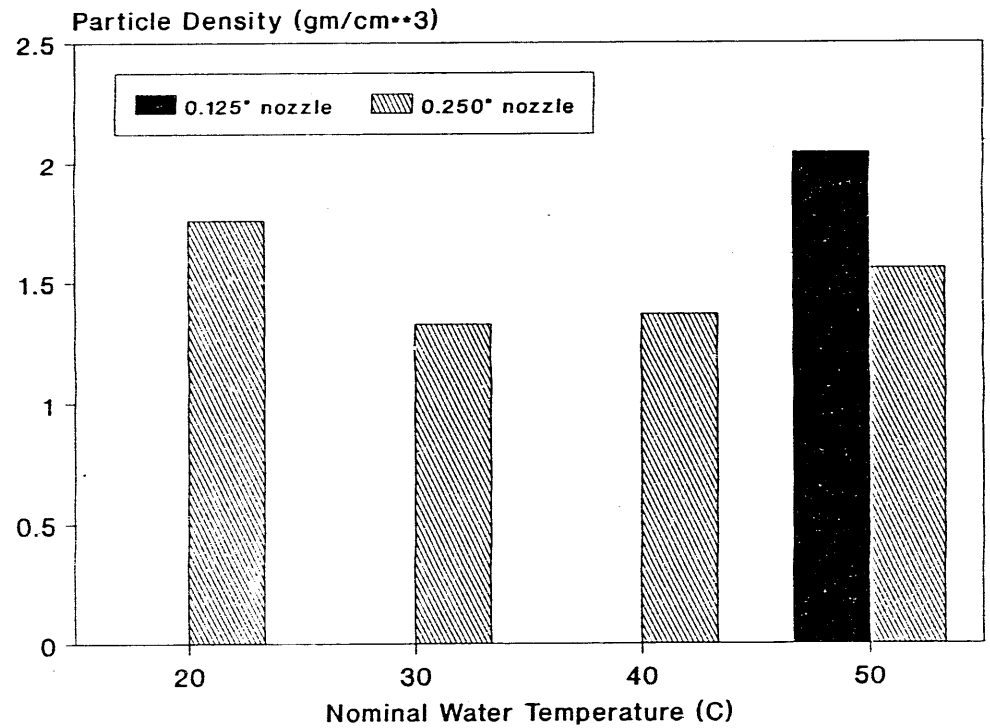

Figure 23. Particle Density vs. Water Temperature for Particles Larger than 1.0 inch.

3.5 Melt Spreading Behavior

All of the tests in which the melt entered the water in the form of a jet experienced jet breakup. However, in tests 10-13, the melt droplets were able to coalesce and reform into a non-fragmented mass at the bottom of the water pool. These tests involved the hottest water pools tested, from 60°C to 70°C, and with one exception, 0.25 in diameter nozzles. The one exception was Run 13 which had a 0.125 inch nozzle; however the water pool was only 25 cm deep which seems to have compensated for the small diameter of the molten jet.

In these tests, heat losses from the jet, and subsequently from the fragmented particles to the heated water pool, were not sufficient to freeze the debris prior to settling out at the bottom of the water pool. The video records of the tests clearly demonstrate that as the drops from the fragmented jet accumulated, they flowed over and into the previously accumulated mass of particles, creating a coherent, structurally rigid formation. These formations were able to be lifted intact from the pool after emptying the pool and are shown in Figures 11-14. Whereas earlier tests (with colder water pools) resulted in a sizable fraction of particulate debris, these tests resulted in no particulate debris at all.

As the melt debris arrived at the submerged floor still molten, it was observed to spread across the steel floor in much the same manner as in our molten aluminum debris spreading tests. This observation was quite surprising; however the spreading behavior does indicate that even these intact debris structures will distribute themselves laterally by spreading under the water, leading to a coolable geometry.

The debris parameters (mass, water temperature and depth, aluminum temperature) were recorded and the average thickness of the spreading formation was compared to the dimensionless spreading correlation previously developed. A comparison of the four data points to the small scale melt spreading correlations previously developed is shown in Figure 24. The lead (Pb) correlation is applicable to oxide or oxidized materials; the aluminum (Al) correlation is applicable to molten metals and, thus, the present data. Comparison of the data to the aluminum melt spreading correlation shows surprisingly good agreement, and suggests that the extent of debris spreading under gamma heating conditions may be estimated by this correlation by application of this correlation for those cases in which the debris does not solidify prior to settling on the tank floor.

3.6 Regimes of Debris Formation Due to Jet Fragmentation and Quenching in Deep Water Pools

During these tests, a wide spectrum of debris sizes and shapes was observed following the quench in the water pool. The different regimes of debris formation were clearly found to change with variation in the experimental parameters; however, no model was available to explain these variations, nor to predict the regime of debris formation apriori. As a result, consideration of phenomena (such as debris coolability) which depend upon the debris morphology could not as yet be put on a firm basis.

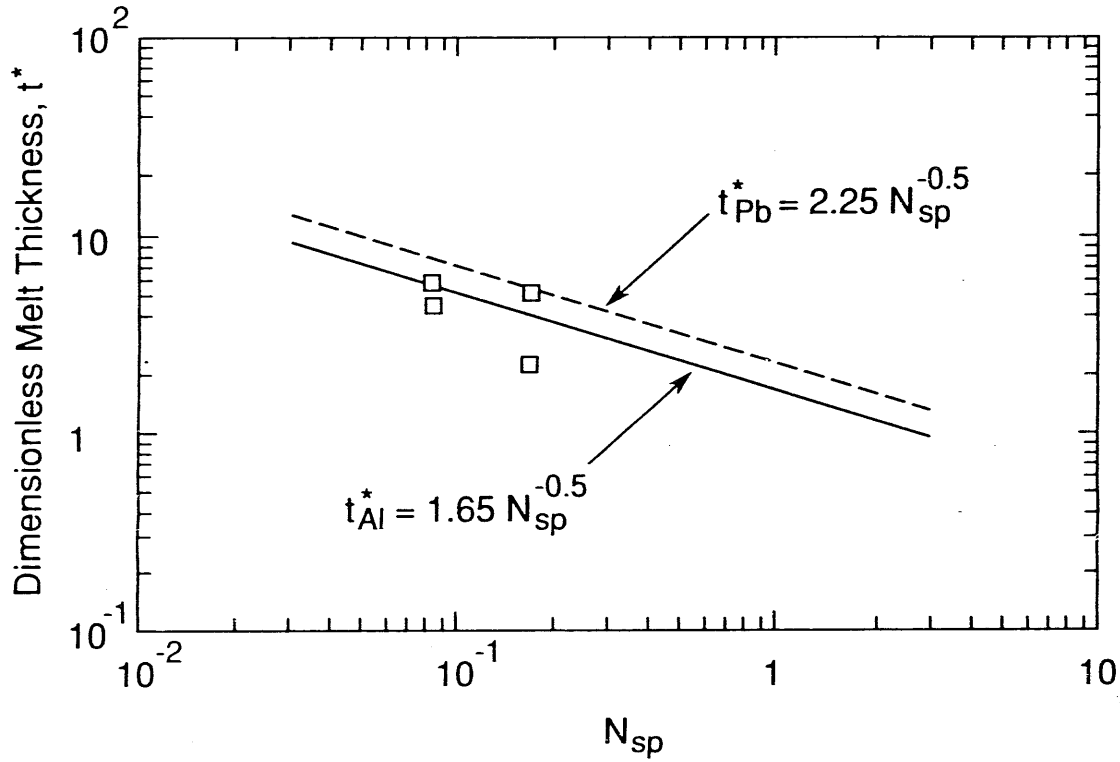

Figure 24. Observed Debris Melt Spreading Behavior for Runs 10-13.

The debris formations that were observed during these experiments have been photographically recorded and are shown in Figures 2-14. They have been characterized according to morphological characteristics which describe the size, shape, and coolability of the debris. The four debris regimes and the tests in which they were observed are listed below.

Regime	Description	Tests
1	Loose debris bed	1
2	Agglomerations of particles	3, 6, 7
3	Tall solid columns	4, 8, 9, 14-18
4	Shallow puddles	10-13

(Note: Runs 2 and 5 have not been included in the regime assessment due to abnormal experimental conditions during their execution).

Specific parameters for these tests as well as characterization of their debris regime are shown in Table 3.

The Regime 1 debris configuration is characterized as a "loose debris bed." As the melt jet enters the water, it fragments into individual particles of spherical-type shape. This regime of debris formation has only been observed in one of the tests, with the coldest water and the smallest nozzle diameter. The cold water and small particle size combine to effect the fastest heat transfer from the particles to the water, freezing them during their descent through the water. The result is a pile of individual particles, much like what you would get from a shot tower, a debris bed of nearly uniform size particles. A pile of particles such as these was found to be easily leveled and, thus, quite easily cooled.

The Regime 2 debris configuration is characterized as "agglomerations of particles" that would have formed a loose debris bed if they did not stick together. In this regime, the melt jet once again fragments into individual particles as was observed for Regime 1. This regime occurred, however, when the water temperature was increased or the melt jet diameter was increased above the values that support Regime 1 formation. Increasing either the water temperature or the melt jet diameter has the effect of reducing the coolability of the individual particles as they settle in a pile at the bottom of the water pool, causing them to stick together in clumps of agglomerated particles instead of the loose bed of particles characteristic of Regime 1. These particles were only weakly held together and they could easily be broken into loose particles. Therefore, it is expected that debris formed in this regime would also behave much like a debris bed of uniform size particles and would be coolable as in Regime 1.

The Regime 3 debris configuration is characterized as a "tall solid column," very much similar to a stalagmite in a cavern. As the melt jet passes through the water, it may or may not fragment into particles. For those tests in which this regime was observed, the water

Table 3 - Regimes and Conditions of Debris Formation

Run	H_w/d_j	T_w (°C)	Debris Regime
1	247	24	1
3	231	40	2
4	253	59	3
6	107	23	2
7	108	31	2
8	110	42	3
9	112	50	3
10	114	61	4
11	119	71	4
12	65	72	4
13	131	71	4
14	60	54	3
15	58	41	3
16	36	40	3
17	36	41	3
18	64	40	3

temperature was in the range 40-60°C and the melt jet was usually 0.25 inch diameter or larger. A cylindrical or conical monolithic structure began to be formed, projecting upward from the floor of the water tank and continuing to grow upwards for the duration of the jet. As the jet material continued to impact upon the growing column, it was observed to be completely molten and was able to flow down the sides of the column, much like a potter adding clay to a mold on a potter's wheel. Examples of the structures so formed are shown in Figures 5, 9 and 10 (Tests 14-18 were not photographically recorded). This regime of debris formation is supported by conditions which tend to limit the heat transfer from the melt jet to the water, i.e. larger jet diameter and/or warmer water temperature than for Regime 2. Although this regime of debris formation is not apparently as coolable as Regimes 1-2, the debris is not mobile and transport of debris into pipes, pumps, assembly inlets, etc. is not a concern. This regime of debris formation would tend to cause molten material to solidify in massive formations around submerged, intact structures, much like water dripping and freezing along the walls of a cold pipe or structure.

The Regime 4 was the last debris configuration that was observed and is characterized as a "shallow puddle" of molten debris that collects in a column, as in Regime 3, but slumps under its own weight and spreads out laterally across the floor under the water. For those tests in which this regime was observed, the water temperature was in the range of 70°C and the melt jet was 0.25 inch diameter. The mound of debris that formed was entirely molten inside and the melt jet was able to penetrate into the molten mound of submerged debris, and exit at the base, spreading under the water. The mound, itself, could not support its own weight and slumped downward like a deflating balloon. Regime 4 created a monolithic structure of debris much like Regime 3; however, in Regime 3 the structure dimension was greatest in the vertical direction while, in Regime 4, the structure dimension was greatest laterally. It seems reasonable to expect that a Regime 3 structure which could not be maintained coolable would slump benignly into a Regime 4 configuration. Examples of Regime 4 structures are shown in Figures 11-14. These formations are immobile due to their large size and, because of their large, upward-facing surface area, would be expected to be quite coolable. A maximum in the surface area for coolability would be approached as the debris spread out to a maximum extent, limited by surface tension of the melt. For molten aluminum under water, this is $t^* = 1$, corresponding to a dimensional thickness of approximately 1 cm.

The single most important consideration in determining which regime of debris formation is likely to be encountered in practice is the coolability of the superheated melt jet as it penetrates downward through the water pool. This in turn is influenced by the depth of the water pool and, most importantly, the water temperature. In order to illustrate these dependencies, the regimes of the various experiments have been plotted in Figure 25 versus the water depth/jet diameter ratio and the water pool temperature. The y-axis indicates the debris regime (height of bar) that was observed (from 1-4); the x-axis is the range of water depth/jet diameter ratio, and the z-axis is the water pool temperature. The dependence upon the depth/diameter ratio is demonstrated by the lateral dependence of the height of the bars; the dependence upon the water pool temperature is demonstrated by the variation in the height of the bars going backward (into the paper). From Figure 25, it is clear that there was only a weak

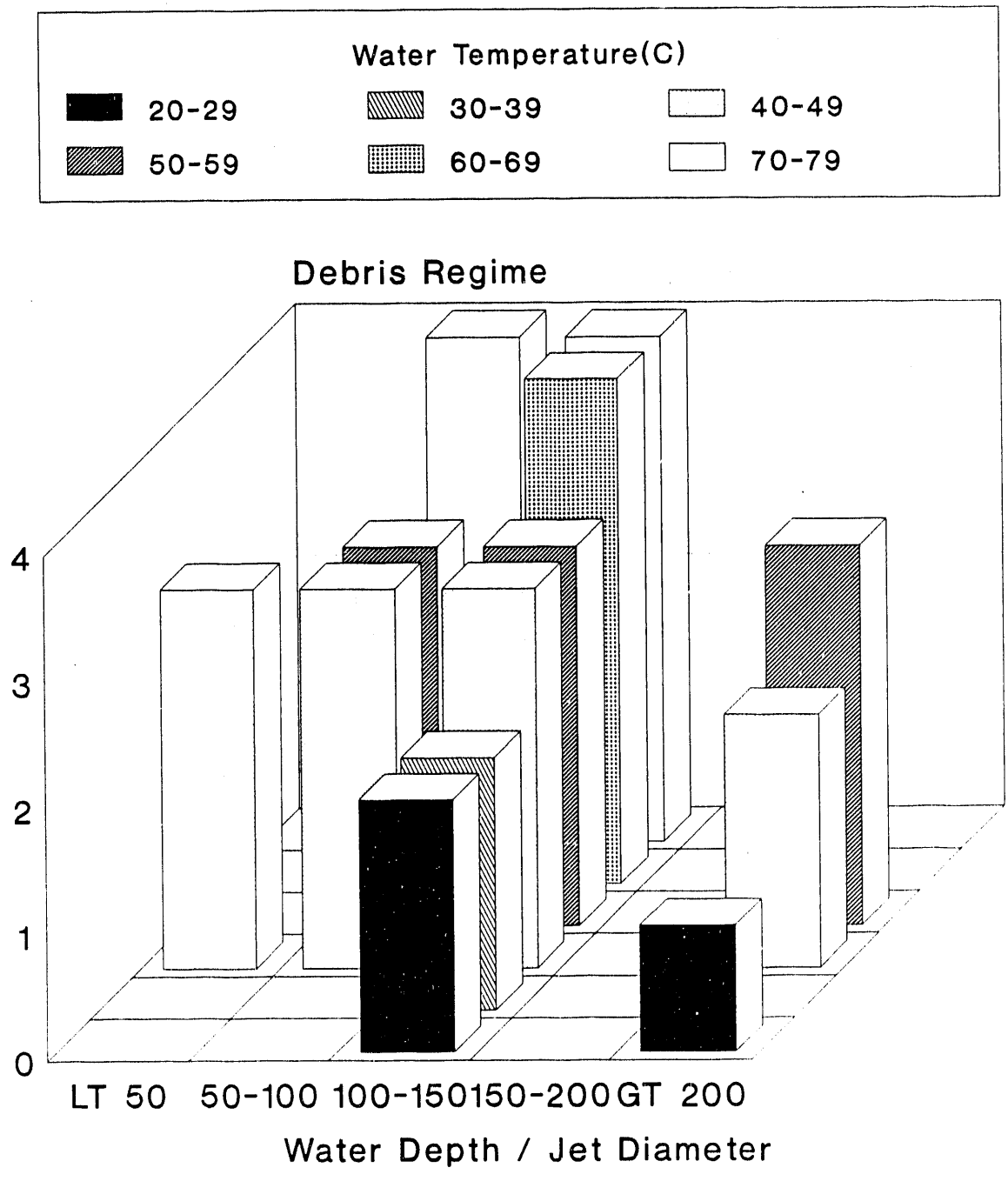

Figure 25. Regimes of Debris Formation Due to Jet Fragmentation and Quenching in Water Pools: (1) Loose debris bed, (2) Agglomerations of particles, (3) Tall solid columns, (4) Shallow puddles.

dependence of the debris formation regime on the water depth/jet diameter ratio. However, the dependence upon the water pool temperature was dominant and is the single most important variable to consider when determining the regime of debris formation. The data matrix in Figure 25 is sparse, many spaces in the matrix do not have data. Additional tests could be performed quite easily to fill in the missing points. Nevertheless, one could make use of this figure in its present form to make technically defensible predictions of the mode of debris formation expected in application.

4. CONCLUSIONS

A series of eighteen experiments were executed in this series of tests to examine the possible interactions as a small diameter jet of molten aluminum penetrates a deep water pool. Of primary interest were the implications with respect to the meltdown of non-fuel components in the reactor tank during γ-heating conditions, in particular the occurrence of aluminum-water steam explosions and the generation of debris from the molten aluminum as it fragments. The following observations and conclusions were made in the course of these investigations:

1. No aluminum-water steam explosions occurred in any of these tests. Other tests with molten aluminum jets at comparable temperatures have been performed with jet diameters up to one inch with a similar result, no explosive interactions.

2. It appears from these tests that the contact mode between aluminum and water is critical in determining whether an aluminum-water steam explosion will occur. These tests employed the jet-entry mode exclusively.

3. The jet breakup length agrees with existing models quite well. Indications are that molten aluminum jets will breakup into large particles even in pools as shallow as one foot deep.

4. In cold water pools, molten aluminum jets break up into particles and form loose debris beds.

5. In hot water pools, the particles from the jet breakup do not completely freeze prior to piling up at the bottom of the pool. There they form clumps of particles and even reform into solid, non-porous formations. These data also suggest a good possibility that melt would refreeze and agglomerate around undamaged components in the portion of the reactor tank below the water line, rendering it immobile.

6. Virtually no particulate debris smaller than 3 mm was formed in these tests.

7. At the highest water pool temperatures, the aluminum melt actually spread radially along the bottom of the pool on the stainless steel base. When correlated according to a correlation developed to predict melt spreading under shallow water pools, the data were in good agreement with the spreading correlation. Debris formations formed in this manner were solid structures.

8. The debris that formed into particles was less dense than solid aluminum. This would make these debris beds easily leveled by crossflow currents, enhancing debris coolability.

5. REFERENCES

Marshall, B. W., Beck, D. F., and Berman, M., "Mixing of Isothermal and Boiling Molten-Core Jets With Water: The Initial Conditions for Energetic FCI's," Proceedings of the International ENS/ANS Conference on Thermal Reactor Safety, Vol. 1, pp. 117-127, Avignon, France, 1988.

Taylor, G. I., "The Dispersion of Jets of Metals of Low Melting Point in Water," 1942, In Batchelor, G. K. "The Scientific Papers of Sir Geoffrey Ingram Taylor: Vol. III, Aerodynamics and the Mechanics of Projectiles and Explosions, Paper 32, Cambridge University Press, Cambridge, MA, 1963.

END

DATE
FILMED
8/11/92